J. Fluid Mech. (1985), *vol.* 158, *pp.* 447–488
Printed in Great Britain

Time-dependent viscous flow past an impulsively started rotating and translating circular cylinder

By H. M. BADR
Mechanical Engineering Department, University of Petroleum and Minerals, Dhahran, Saudi Arabia

AND S. C. R. DENNIS
Department of Applied Mathematics, University of Western Ontario, London, Ontario, Canada

(Received 6 April 1983 and in revised form 12 February 1985)

A numerical study is made of the development with time of the two-dimensional flow of a viscous, incompressible fluid around a circular cylinder which suddenly starts rotating about its axis with constant angular velocity and translating at right angles to this axis with constant speed. The governing partial differential equations in two space variables and time are reduced to sets of time-dependent equations in one space variable by means of Fourier analysis. By truncating the Fourier series to a finite number of terms, a finite set of differential equations is solved to give an approximation to the theoretical flow. The solutions are obtained by numerical methods. Results are given for the initial development with time of the asymmetrical wake at the rear of the cylinder at Reynolds numbers $R \geqslant 200$, based on the diameter of cylinder, and at small rotation rates. The detailed results show the formation of a Kármán vortex street. The time development of this separated flow is compared in detail at $R = 200$ with recent experimental results. The details of the formation and movement of the vortices behind the cylinder and the velocity profiles in several locations are virtually identical in the experimental and theoretical studies. The variations with time of the lift, drag and moment exerted by the fluid on the cylinder are determined both by calculations and by means of approximate analytical expressions. The agreement between these results at small times is excellent.

1. Introduction

Unsteady flow around a cylinder which is suddenly started from rest in a viscous fluid has long been of interest both experimentally and theoretically. Many properties of such flows are described in standard works such as Prandtl & Tietjens (1934) and Batchelor (1970) and details of recent work are given by Telionis (1981). In the present paper we shall study the two-dimensional flow generated by an infinitely long circular cylinder of cross-sectional radius a which translates with uniform velocity U at right angles to its axis and rotates about this axis with constant angular velocity ω_0. A frame of reference which translates with the cylinder but does not rotate is employed and the motion is assumed to be governed by the Navier–Stokes equations for incompressible fluids. It is further supposed that the uniform translation and rotation of the cylinder start impulsively at the same instant. There are two basic parameters in the problem. One is the Reynolds number, defined as $R = 2Ua/\nu$, where ν is the coefficient of kinematic viscosity of the fluid. The second is the parameter $\alpha = a\omega_0/U$, which is a dimensionless measure of the speed of rotation of a point on

the surface of the cylinder relative to its speed of translation. When $\alpha = 0$ the motion is symmetrical about the direction of translation; this case has received a considerable amount of previous attention.

When α is non-zero many important effects which are otherwise absent appear. These include the production of a lift force and moment on the cylinder and a circulation around it. Tollmein (1924) investigated the initial flow following an impulsive start in such a case by an extension of the results of boundary-layer theory used by Blasius (1908) in the symmetrical case $\alpha = 0$. The first terms of an expansion in powers of the time were obtained. This expansion was later developed further for the case $\alpha = 0$ by Goldstein & Rosenhead (1936) but this non-zero-α case does not appear to have been considered. Some attention is given to the expansion method in the present paper following the methods of Collins & Dennis (1973*a*) for the case $\alpha = 0$.

The majority of the investigations so far made for non-zero α are for the problem of steady flow. For this problem there is associated with each value of α a circulation round a sufficiently large contour surrounding the cylinder which may not exist in the unsteady flow until sufficient time has elapsed for circulation to diffuse across the contour from the cylinder. Glauert (1957*a*, *b*) considered the steady flow for high R and both large and small values of α on the basis of boundary-layer theory and was able to correlate the circulation round a contour at the edge of the boundary layer with α. Wood (1957) and Moore (1957) obtained results generally consistent with those of Glauert from their steady-state theoretical work. Moore (1957) investigated the problem for large α and finite Reynolds numbers. In all of these investigations it was possible to determine the lift on the cylinder, which was found to increase with α.

There has also been a small amount of numerical work in the case of steady flow past a rotating circular cylinder. The earliest numerical solutions of the Navier–Stokes equations for non-zero α were given by Thoman & Szewczyk (1966). More recent calculations were given by Ta Phuoc Loc (1975) at $R = 5$ and 20 by solving the Navier–Stokes equations numerically within a finite region surrounding the cylinder subject to a boundary condition on the perimeter of the region chosen to be consistent with external potential flow. Results for the steady-state flow field were obtained together with values of the lift and drag coefficients for small values of α. Ingham (1983) has reconsidered the numerical solution for the same cases $R = 5$ and 20 with $0 \leqslant \alpha \leqslant 0.5$ using several possible boundary conditions at finite but large enough distances from the cylinder. The calculated streamline patterns were similar to those of Ta Phuoc Loc (1975) but there were considerable discrepancies in the lift and drag coefficients. Moreover, Ingham's own calculated lift coefficients vary considerably with the form of external boundary condition assumed, particularly for $\alpha = 0.5$, with a lesser but noticeable corresponding variation in the drag coefficient.

The unsteady development of flow past a rotating circular cylinder is of interest for several theoretical reasons. In the first place it may give some insight into the phenomenon of unsteady separation in which, following the sudden start of the motion from rest, a recirculating region develops within the attached boundary layer on the cylinder surface, eventually followed by breakaway of this region to form a recirculating wake. The situation has been discussed theoretically by Riley (1975) in a general way. In the present problem separation occurs from the moving wall when α is non-zero in a more complicated way than when $\alpha = 0$ and the condition for separation is not the simple condition of vanishing wall-shear stress. Unsteady separation has been discussed by Sears & Telionis (1975), who proposed that the model

based on the original work of Rott (1956), Sears (1956) and Moore (1958) is appropriate. In this model the point of separation is defined as the point where both the skin friction and the fluid velocity become zero within the attached boundary layer as it appears to an observer moving with the separation. Sears & Telionis (1975) and Williams (1977) have attempted to substantiate this criterion; they indicate the velocity profiles and streamlines to be expected at separation. Inoue (1981) has discussed the differences between unsteady separation at walls moving in the upstream and downstream directions and suggests that the separation criterion of Rott (1956), Sears (1956) and Moore (1958) appears to be satisfied for downstream-moving walls, but for upstream-moving walls there are cases in which it does not seem to hold. In the present problem we have both upstream- and downstream-moving walls on account of the rotation of the cylinder relative to the translating frame of reference.

One of the essential objects of the present study is to obtain numerical solutions of the Navier–Stokes equations which can be correlated not only with theoretical studies but also with available experimental data. Experimental studies of various steady and unsteady flows related to the present problem have been given by Prandtl (1925), Prandtl & Tietjens (1934), Ludwig (1964), Taneda (1977) and Koromilas & Telionis (1980), but by far the most extensive work of relevance is the recent study of Coutanceau & Ménard (1985). In these experiments a circular cylinder starts rotating and translating at the same instant at constant rates of rotation and translation which are maintained during the subsequent motion. The development of the motion with time is observed for various values of $R \geqslant 200$ and for $\alpha \leqslant 3.5$ using visualization techniques which follow previous work of Coutanceau & Bouard (1977*a*, *b*) and Bouard & Coutanceau (1980) in the case $\alpha = 0$.

In the present paper numerical solutions of the Navier–Stokes equations are obtained under the same conditions as the experimental study of Coutanceau & Ménard (1985). The numerical techniques employed are a direct extension of those which were used by Collins & Dennis (1973*a*, *b*) in the case $\alpha = 0$. Modified polar coordinates (ξ, θ), where $\xi = \ln(r/a)$ in terms of the radial distance r, are taken with the origin at the centre of the cylinder in the translating frame. The stream function and scalar vorticity are used as dependent variables. The two equations governing these functions are reduced to sets of partial differential equations in the variable ξ and the time by employing Fourier series expansions in the angular coordinate θ. An approximation to the flow is then obtained by solving a finite number of these equations. The Fourier series are full-range series in $0 \leqslant \theta \leqslant 2\pi$ rather than the half-range series in $0 \leqslant \theta \leqslant \pi$ employed by Collins & Dennis for the symmetrical case $\alpha = 0$. Full-range Fourier series have previously been used by Dennis & Staniforth (1971), Staniforth (1973) and Patel (1981) in formulating numerical techniques for solving problems with no special symmetry properties in $0 \leqslant \theta \leqslant 2\pi$. A preliminary account of the method in the present problem was given by Badr & Dennis (1981).

The present calculations are confined to the small rotation rates $\alpha = \frac{1}{2}$ and 1. Here the interaction between the effects of rotation and translation is relatively small and it is possible to achieve accurate results without excessive computational labour. Detailed results are given for $R = 200$ and 500; in both cases the calculations exhibit the early stages of the formation of a Kármán vortex street. Such an occurrence is not new in numerical solutions. A Kármán vortex street was, for example, generated by Patel (1981) in his study of flow past an elliptic cylinder. The new point in the present results is the exceptionally good quantitative comparisons with the experimental results of Coutanceau & Ménard at $R = 200$, not only in the detailed

formation of the wake but also in the development with time of velocity profiles and various other properties of the flow. In fact, the general evidence of the comparisons is that the experimental and numerical treatments of the problem in this case are virtually identical and give the same physical development of the flow in every respect.

2. Governing equations and method of solution

At time $t = 0$, an infinitely long circular cylinder suddenly starts to move in a viscous, incompressible fluid with constant speed U at right angles to its axis and at the same instant starts to rotate about its axis with constant angular velocity ω_0. A suitable frame of reference is used in which axes translating with the cylinder but fixed in direction are taken in the plane of a circular cross-section with origin 0 at the centre. Modified polar coordinates (ξ, θ) are used, where $\xi = \ln(r/a)$ and a is the radius of the cylinder. Thus the cylinder is situated at $\xi = 0$ and the domain of the solution is $\xi \geqslant 0$, $0 \leqslant \theta \leqslant 2\pi$, with $\theta = 0$ in the downstream direction.

The motion is two-dimensional and may be described in terms of the usual two simultaneous equations satisfied by the stream function and the scalar vorticity. Dimensionless functions ψ and ζ are used, related to the dimensional stream function ψ^* and scalar vorticity ζ^* by the equations $\psi^* = Ua\psi$, $\zeta^* = -U\zeta/a$. The dimensionless radial and transverse components of velocity (u, v) obtained by dividing the actual components by U are then given by

$$u = e^{-\xi}\frac{\partial \psi}{\partial \theta}, \quad v = -e^{-\xi}\frac{\partial \psi}{\partial \xi}, \tag{1}$$

and the function ζ is defined by

$$\zeta = e^{-\xi}\left(\frac{\partial u}{\partial \theta} - \frac{\partial v}{\partial \xi} - v\right). \tag{2}$$

The equations of motion can be expressed as the two equations

$$e^{2\xi}\frac{\partial \zeta}{\partial \tau} = \frac{2}{R}\left(\frac{\partial^2 \zeta}{\partial \xi^2} + \frac{\partial^2 \zeta}{\partial \theta^2}\right) - \frac{\partial \psi}{\partial \theta}\frac{\partial \zeta}{\partial \xi} + \frac{\partial \psi}{\partial \xi}\frac{\partial \zeta}{\partial \theta}, \tag{3}$$

$$\frac{\partial^2 \psi}{\partial \xi^2} + \frac{\partial^2 \psi}{\partial \theta^2} = e^{2\xi}\zeta. \tag{4}$$

Here $\tau = Ut/a$ and R is the Reynolds number defined by $R = 2aU/\nu$, where ν is the coefficient of kinematic viscosity.

Equations (3) and (4) are those considered by Collins & Dennis (1973*a*, *b*) in the case of sudden translation of a circular cylinder without rotation. Here the rotation of the cylinder enters through the parameter $\alpha = a\omega_0/U$ in the boundary conditions, which may be stated as

$$\psi = 0, \quad \frac{\partial \psi}{\partial \xi} = -\alpha \quad \text{when} \quad \xi = 0, \tag{5}$$

and

$$e^{-\xi}\frac{\partial \psi}{\partial \xi} \to \sin\theta, \quad e^{-\xi}\frac{\partial \psi}{\partial \theta} \to \cos\theta \quad \text{as} \quad \xi \to \infty. \tag{6}$$

The sets of conditions (5) and (6) must be satisfied for all θ such that $0 \leqslant \theta \leqslant 2\pi$ and,

moreover, all of the dependent variables in the flow domain must be periodic functions of θ with period 2π. Thus, in particular,

$$\psi(\xi,\theta+2\pi,\tau)=\psi(\xi,\theta,\tau);\quad \zeta(\xi,\theta+2\pi,\tau)=\zeta(\xi,\theta,\tau). \tag{7}$$

In the case $\alpha=0$ considered by Collins & Dennis (1973*a*, *b*) the motion is symmetrical about $\theta=0$, $\theta=\pi$. Then the functions ψ and ζ are odd functions of θ which vanish on $\theta=0,\pi$. Here the problem is more complicated because, although the conditions (7) ensure that the velocity components u and v are also periodic functions of θ with period 2π, care must be exercised to ensure that the pressure in the fluid is likewise periodic in θ; this will be considered shortly.

Collins & Dennis (1973*a*, *b*) used Fourier-series substitutions for ψ and ζ to reduce (3) and (4) to sets of partial differential equations in ξ and τ. These were solved by exact analysis for small values of τ (1973*a*) and by numerical methods for larger values of τ (1973*b*). In the present case the Fourier series are of the form

$$\psi(\xi,\theta,\tau)=\tfrac{1}{2}F_0(\xi,\tau)+\sum_{n=1}^{\infty}\{F_n(\xi,\tau)\cos n\theta+f_n(\xi,\tau)\sin n\theta\}, \tag{8a}$$

$$\zeta(\xi,\theta,\tau)=\tfrac{1}{2}G_0(\xi,\tau)+\sum_{n=1}^{\infty}\{G_n(\xi,\tau)\cos n\theta+g_n(\xi,\tau)\sin n\theta\}. \tag{8b}$$

The equations governing the various functions in (8) are obtained by substitution in (3) and (4). It is found from (4) that

$$\frac{\partial^2 F_n}{\partial\xi^2}-n^2F_n=e^{2\xi}G_n\quad(n=0,1,2,\ldots). \tag{9a}$$

and

$$\frac{\partial^2 f_n}{\partial\xi^2}-n^2f_n=e^{2\xi}g_n\quad(n=1,2,\ldots). \tag{9b}$$

Boundary conditions for (9) follow from (5) and (6). They are that at the cylinder surface

$$F_0(0,\tau)=0;\quad F_n(0,\tau)=f_n(0,\tau)=0\quad(n=1,2,\ldots), \tag{10a}$$

$$\frac{\partial F_0}{\partial\xi}=-2\alpha;\quad \frac{\partial F_n}{\partial\xi}=\frac{\partial f_n}{\partial\xi}=0\quad\text{when}\quad\xi=0\quad(n=1,2,\ldots), \tag{10b}$$

and as $\xi\to\infty$

$$e^{-\xi}F_0\to0;\quad e^{-\xi}F_n\to0,\quad e^{-\xi}f_n\to\delta_n\quad(n=1,2,\ldots), \tag{11a}$$

$$e^{-\xi}\frac{\partial F_0}{\partial\xi}\to0;\quad e^{-\xi}\frac{\partial F_n}{\partial\xi}\to0,\quad e^{-\xi}\frac{\partial f_n}{\partial\xi}\to\delta_n\quad(n=1,2,\ldots), \tag{11b}$$

where

$$\delta_1=1;\quad\delta_n=0\quad(n=2,3,\ldots). \tag{12}$$

It also follows from (6) that as $\xi\to\infty$

$$G_0\to0;\quad G_n\to0,\quad g_n\to0\quad(n=1,2,\ldots). \tag{13}$$

The conditions (13) are required in the numerical solution of (3) and it may now be shown, following Collins & Dennis (1973*a*, *b*), that (10) and (11) can be combined

to give further sets of conditions on the functions G_n and g_n to be used in solving the sets of equations derived from (3). The conditions are

$$\int_0^\infty e^{2\xi} G_0(\xi,\tau)\,d\xi = 2\alpha, \tag{14a}$$

$$\left.\begin{aligned}\int_0^\infty e^{(2-n)\xi} G_n(\xi,\tau)\,d\xi &= 0, \qquad (14b)\\ \int_0^\infty e^{(2-n)\xi} g_n(\xi,\tau)\,d\xi &= 2\delta_n \qquad (14c)\end{aligned}\right\} \quad (n = 1,2,\ldots),$$

where δ_n has the significance in (12). The sets of equations (14*b*, *c*) are obtained by multiplying (9), excluding $n = 0$, by $e^{-n\xi}$ and integrating both sides from $\xi = 0$ to $\xi = \infty$. The results readily follow after some integration by parts of the term involving the second derivative on the left-hand side of each typical equation together with use of the conditions (10) and (11). The result (14*a*) further follows directly from the application of this procedure to the member of (9*a*) with $n = 0$ and it is merely an expression of the fact that the circulation round a large enough contour surrounding the cylinder must vanish for all time. Some further discussion of this point is worthwhile in view of the numerical procedure adopted in the present paper.

The motion is started suddenly from rest; thus the initial circulation round a circular contour centred at the cylinder and of large enough radius $\xi = \xi_m$ is zero. If we evaluate the circulation $\kappa(\xi_m,\tau)$ round this contour using (8*a*) then $\kappa = -\pi(\partial F_0/\partial\xi)_{\xi=\xi_m}$ and it follows that $\partial F_0/\partial\xi = 0$ for $\xi \geqslant \xi_m$, where ξ_m defines the contour. Thus (14*a*) is established for any value of τ and we can replace the upper limit by ξ_m at any τ for which no vorticity has yet passed across $\xi = \xi_m$. Moreover, the satisfaction of (14*a*) is the required condition to ensure that the pressure in the fluid is periodic with period 2π in θ. We substitute (8) in (3) and integrate with respect to θ from $\theta = 0$ to $\theta = 2\pi$, which gives

$$e^{2\xi}\frac{\partial G_0}{\partial\tau} = \frac{2}{R}\frac{\partial^2 G_0}{\partial\xi^2} + \sum_{n=1}^{\infty}\frac{\partial}{\partial\xi}\{n(F_n g_n - f_n G_n)\}. \tag{15}$$

If now

$$I(\xi,\tau) = \int_0^\xi e^{2z} G_0(z,\tau)\,dz \tag{16}$$

and it is assumed that the summation in (15) vanishes as $\xi \to \infty$ by (13), integration of (15) from $\xi = 0$ to $\xi = \infty$ gives

$$\left(\frac{\partial I}{\partial\tau}\right)_{\xi=\infty} = -\frac{2}{R}G_0'(0,\tau). \tag{17}$$

Now if $p(\xi,\theta,\tau)$ denotes the pressure in the fluid and $p_0(\theta,\tau)$ denotes its value at $\xi = 0$ it is easily shown that

$$\frac{p_0(\theta,\tau) - p_0(0,\tau)}{\frac{1}{2}\rho U^2} = -\frac{4}{R}\int_0^\theta \left(\frac{\partial\xi}{\partial\xi}\right)_{\xi=0} d\theta,$$

and hence that

$$p_0(2\pi+\theta,\tau) - p_0(\theta,\tau) = -\frac{2\pi\rho U^2}{R}G_0'(0,\tau), \tag{18}$$

for all values of θ.

It follows that, provided (14*a*) is satisfied for all τ, i.e. that there is never any circulation round a sufficiently large contour, and that (15) is satisfied along with all the necessary boundary conditions, then

$$G_0'(0,\tau) = 0 \tag{19}$$

for all τ and consequently from (18) the surface pressure remains periodic. Since the pressure at any point in the fluid can be obtained from the surface pressure by integration of the component momentum equation in the radial direction and ψ, ζ have themselves been determined to be periodic in θ with period 2π, it follows that the pressure is everywhere periodic with period 2π. All the conditions of the problem are therefore satisfied. In this sense we consider the satisfaction of (14) as a very important part of the solution procedure. The condition (14*a*) must be satisfied to ensure that the circulation round a large contour is zero; the conditions (14*b*, *c*) ensure that the free stream is approached far from the cylinder, just as the satisfaction of (14*c*) gave this assurance in the symmetrical case considered by Collins & Dennis (1973*a*, *b*).

Equation (15) gives the equation to be satisfied by the function $G_0(\xi,\tau)$, and the sets of equations satisfied by $G_n(\xi,\tau)$ and $g_n(\xi,\tau)$ for general integer values of n are obtained by substitution of (8) into (3), multiplication by $\cos n\xi$ or $\sin n\xi$ respectively, and integration from $\theta = 0$ to $\theta = 2\pi$. The sets of equations which result are

$$e^{2\xi}\frac{\partial G_n}{\partial \tau} = \frac{2}{R}\left(\frac{\partial^2 G_n}{\partial \xi^2} - n^2 G_n\right) - \tfrac{1}{2}nf_n\frac{\partial G_0}{\partial \xi} + \tfrac{1}{2}S_n, \tag{20a}$$

$$e^{2\xi}\frac{\partial g_n}{\partial \tau} = \frac{2}{R}\left(\frac{\partial^2 g}{\partial \xi^2} - n^2 g_n\right) + \tfrac{1}{2}nF_n\frac{\partial G_0}{\partial \xi} + \tfrac{1}{2}T_n, \tag{20b}$$

where

$$S_n = \sum_{m=1}^{\infty}\left[\{(m-n)F_j + kF_k\}\frac{\partial g_m}{\partial \xi} - \{jf_j + kf_k\}\frac{\partial G_m}{\partial \xi} + m\left\{\frac{\partial F_j}{\partial \xi} + \frac{\partial F_k}{\partial \xi}\right\}g_m - m\left\{\operatorname{sgn}(m-n)\frac{\partial f_j}{\partial \xi} + \frac{\partial f_k}{\partial \xi}\right\}G_m\right], \tag{21a}$$

$$T_n = \sum_{m=1}^{\infty}\left[(kf_k - jf_j)\frac{\partial g_m}{\partial \xi} - \{(m-n)F_j - kF_k\}\frac{\partial G_m}{\partial \xi} - m\left\{\operatorname{sgn}(m-n)\frac{\partial f_j}{\partial \xi} - \frac{\partial f_k}{\partial \xi}\right\}g_m - m\left(\frac{\partial F_j}{\partial \xi} - \frac{\partial F_k}{\partial \xi}\right)G_m\right], \tag{21b}$$

and, in (21*a*, *b*), $j = |m-n|$, $k = m+n$ and $\operatorname{sgn}(m-n)$ is the sign of $(m-n)$ with $\operatorname{sgn}(0) = 0$. This completes the theoretical description of the method of solution using the independent variables ξ, θ, τ. In theory one has to solve the sets of equations (9), (15) and (20) which are infinite in number; in practice one has to solve sufficient of them to give a satisfactory approximation to the flow. The boundary conditions for (9) are the sets of initial conditions (10). For (15) and (20) they are the conditions (13) and (14). The latter conditions ensure that the external-flow conditions (11) are satisfied and that the circulation round a contour surrounding the cylinder and with all points of it at infinite distance from the cylinder remains zero.

3. Determination of the initial flow

The initial flow is governed by the usual boundary-layer theory in which a layer of thickness $(\tau/R)^{\frac{1}{2}}$ surrounds the cylinder following the sudden start. We therefore introduce variables appropriate to this layer defined by

$$\xi = \lambda z; \quad \lambda = 2\left(\frac{2\tau}{R}\right)^{\frac{1}{2}}, \tag{22}$$

and then transform all the appropriate equations using (22) together with the scalings of variables

$$f_n = \lambda f_n^*, \quad g_n = \frac{g_n^*}{\lambda} \quad (n = 1, 2, \ldots); \tag{23a}$$

$$F_n = \lambda F_n^*, \quad G_n = \frac{G_n^*}{\lambda} \quad (n = 0, 1, 2, \ldots). \tag{23b}$$

The equations (9) then become (suppressing all stars)

$$\frac{\partial^2 F_n}{\partial z^2} - n^2\lambda^2 F_n = \mathrm{e}^{2\lambda z} G_n \quad (n = 0, 1, 2, \ldots); \tag{24a}$$

$$\frac{\partial^2 f_n}{\partial z^2} - n^2\lambda^2 f_n = \mathrm{e}^{2\lambda z} g_n \quad (n = 1, 2, \ldots); \tag{24b}$$

while (20) become

$$\mathrm{e}^{-2\lambda z}\frac{\partial^2 G_n}{\partial z^2} + 2z\frac{\partial G_n}{\partial z} + 2G_n = 4\tau\frac{\partial G_n}{\partial \tau} + \mathrm{e}^{-2\lambda z}\lambda^2 n^2 G_n + 2\mathrm{e}^{-2\lambda z}\tau n f_n\frac{\partial G_0}{\partial z} - 2\tau\,\mathrm{e}^{-2\lambda z} S_n \quad (n = 1, 2, \ldots); \tag{25a}$$

$$\mathrm{e}^{-2\lambda z}\frac{\partial^2 g_n}{\partial z^2} + 2z\frac{\partial g_n}{\partial z} + 2g_n = 4\tau\frac{\partial g_n}{\partial \tau} + \mathrm{e}^{-2\lambda z}\lambda^2 n^2 g_n - 2\,\mathrm{e}^{-2\lambda z}\tau n F_n\frac{\partial G_0}{\partial z} - 2\tau\,\mathrm{e}^{-2\lambda z} T_n \quad (n = 1, 2, \ldots). \tag{25b}$$

Here S_n and T_n are simply (21) with ξ replaced by z and all unstarred functions f_n, g_n, F_n, G_n replaced by starred functions f_n^*, g_n^*, F_n^*, G_n^* respectively.

The boundary conditions utilized in conjunction with (24) and (25) are the transformed conditions (10) and (14) after (22) and (23) have been applied. This gives

$$\left.\begin{aligned} &F_0(0,\tau) = 0; \quad F_n(0,\tau) = f_n(0,\tau) = 0 \quad (n = 1, 2, \ldots); \\ &\frac{\partial F_0}{\partial z} = -2\alpha; \quad \frac{\partial F_n}{\partial z} = \frac{\partial f_n}{\partial z} = 0 \quad \text{when } z = 0 \quad (n = 1, 2, \ldots) \end{aligned}\right\} \tag{26}$$

and

$$\left.\begin{aligned} &\int_0^\infty \mathrm{e}^{2\lambda z} G_0(z,\tau)\,\mathrm{d}z = 2\alpha, \\ &\int_0^\infty \mathrm{e}^{(2-n)\lambda z} G_n(z,\tau)\,\mathrm{d}z = 0, \\ &\int_0^\infty \mathrm{e}^{(2-n)\lambda z} g_n(z,\tau)\,\mathrm{d}z = 2\delta_n \end{aligned}\right\} \quad (n = 1, 2, \ldots). \tag{27}$$

With these conditions it is possible to construct a numerical method of solution of (24) and (25) for small values of τ. It follows closely the method described by Collins & Dennis (1973*b*) in the symmetrical case $\alpha = 0$ and will be briefly summarized later. It is also possible to develop an exact solution in powers of τ following the method of Collins & Dennis (1973*a*). For small values of τ this series solution can be used to check the numerical integrations, so we shall now give some details.

If we put $\tau = \lambda = 0$ for the start of the motion, (25) give

$$\frac{\partial^2 G_n}{\partial z^2} + 2z\frac{\partial G_n}{\partial z} + 2G_n = 0; \quad \frac{\partial^2 g_n}{\partial z^2} + 2z\frac{\partial g_n}{\partial z} + 2g_n = 0. \tag{28a,b}$$

The solutions of these equations satisfying (27) are

$$\left.\begin{aligned} G_0(z,0) &= \frac{4\alpha}{\pi^{\frac{1}{2}}}\,\mathrm{e}^{-z^2}, \quad G_n(z,0) \equiv 0 \quad (n \neq 0); \\ g_n(z,0) &= \frac{4}{\pi^{\frac{1}{2}}}\,\delta_n\,\mathrm{e}^{-z^2}; \end{aligned}\right\} \tag{29}$$

which yields the expression (for the starred function corresponding to (23))

$$\zeta(z,\theta,0) = 2\pi^{-\frac{1}{2}}(\alpha + 2\sin\theta)\,\mathrm{e}^{-z^2}. \tag{30}$$

The corresponding solutions to (24) obtained using (29) are easily found as

$$\left.\begin{aligned} F_0 &= -2\alpha[z(1-\operatorname{erf} z) + \pi^{-\frac{1}{2}}(1-\mathrm{e}^{-z^2})], \\ F_n &\equiv 0, \\ f_n &= 2[z\operatorname{erf} z - \pi^{-\frac{1}{2}}(1-\mathrm{e}^{-z^2})]\,\delta_n, \end{aligned}\right\} \tag{31}$$

which gives the initial expression for $\psi(z,\theta,0)$.

From the initial expressions (29) and (31) we may now build up a perturbation solution in powers of τ following Collins & Dennis (1973*a*). The expansions for the stream function and vorticity can be made in terms of both λ and τ. In the first place we may expand ψ and ζ in the form

$$\psi = \psi_0 + \lambda\psi_1 + \lambda^2\psi_2 + \ldots, \quad \zeta = \zeta_0 + \lambda\zeta_1 + \lambda^2\zeta_2 + \ldots, \tag{32a, b}$$

where $\psi_m \equiv \psi_m(z,\theta,\tau)$, $\zeta_m \equiv \zeta_m(z,\theta,\tau)$. Then each ψ_m, ζ_m is expanded as a series of powers of τ in the form

$$\psi_m(z,\theta,\tau) = \sum_{n=0}^{\infty} \psi_{mn}(z,\theta)\,\tau^n, \quad \zeta_m(z,\theta,\tau) = \sum_{n=0}^{\infty} \zeta_{mn}(z,\theta)\,\tau^n, \tag{33a, b}$$

where each of the coefficients ψ_{mn}, ζ_{mn} consists of combinations of functions of z with periodic functions of θ. The process of derivation of these coefficients follows very closely the procedures described by Collins & Dennis (1973*a*). It is not necessary to give the analysis in detail and we shall give only the expressions which have been derived for a few of the functions in the series in (33). The process of deriving analyticial expressions soon becomes quite complicated. Thus only the leading terms involved in (33) are obtained in order to check the numerical integration procedure of solving (24) and (25) at small values of τ. This numerical integration procedure gives a much more efficient way of calculating the flow as τ increases.

We can set up equations for the functions $\psi_{mn}(z,\theta)$, $\zeta_{mn}(z,\theta)$ by following the procedures used by Collins & Dennis (1973*a*) and similarly deduce boundary conditions to be satisfied by these functions. In practice each of these functions can

be decomposed into a finite set of Fourier components in the coordinate θ with coefficients which are functions of the variable z. The differential equations to be satisfied by the functions of z are easily found and the boundary conditions which these functions satisfy are deduced from (26) and (27). In other words, each of the Fourier coefficients appearing in (26) and (27) may be considered as a function of z, τ and also to be dependent on λ. On expansion in powers of τ and λ and equating to zero each coefficient of $\lambda^m \tau^n$, we get the conditions which the Fourier components must satisfy. In the following we shall identify only the composite functions.

The leading terms ζ_{00} and ψ_{00} of the expansions are given by means of (30) and (31). From these, following closely the analysis of Collins & Dennis (1973*a*), it is found that ζ_{01} satisfies the equation

$$\frac{\partial^2 \zeta_{01}}{\partial z^2} + 2z \frac{\partial \zeta_{01}}{\partial z} - 2\zeta_{01} = r_1(z) \cos\theta + r_2(z) \sin 2\theta, \tag{34}$$

where $$r_1(z) = -16\alpha\pi^{-\frac{1}{2}} \mathrm{e}^{-z^2} [(2z^2+1) \operatorname{erf} z + 2\pi^{-\frac{1}{2}} z \, (\mathrm{e}^{-z^2} - 1) - 1],$$

and $$r_2(z) = -16\pi^{-\frac{1}{2}} [(2z^2+1) \operatorname{erf} z + 2\pi^{-\frac{1}{2}} z \, (\mathrm{e}^{-z^2} - 1)] \, \mathrm{e}^{-z^2}.$$

The solution satisfying all the boundary conditions is

$$\zeta_{01} = \alpha[L(z) - 8z(1 - \operatorname{erf} z) + 4\pi^{-\frac{1}{2}} \mathrm{e}^{-z^2}] \cos\theta + L(z) \sin 2\theta,$$

where

$$L(z) = A[\mathrm{e}^{-z^2} + \pi^{\frac{1}{2}} z \operatorname{erf} z] + Bz - 4z \operatorname{erf}^2 z + \tfrac{4}{3}\pi^{-1} z[3\,\mathrm{e}^{-z^2} - 4] \, \mathrm{e}^{-z^2} + 2\pi^{-\frac{1}{2}} (2z^2 - 1) \, \mathrm{e}^{-z^2} \operatorname{erf} z,$$

and $$A = -4\pi^{-\frac{1}{2}} (1 + \tfrac{4}{3}\pi^{-1}), \quad B = 8(1 + \tfrac{2}{3}\pi^{-1}).$$

Thus if R is large enough and τ small, the solution is given approximately by

$$\zeta \sim \zeta_{00} + \tau \zeta_{01}. \tag{35}$$

The corresponding surface vorticity is given by

$$\zeta(0, \theta, \tau) \sim 2\pi^{-\frac{1}{2}} (\alpha + 2 \sin\theta) - [\tfrac{16}{3}\pi^{-\frac{3}{2}} \alpha \cos\theta - A \sin 2\theta] \, \tau. \tag{36}$$

The stream function can be obtained corresponding to (35) by integrating $\partial^2 \psi / \partial z^2 = \zeta$ twice subject to $\psi = \partial \psi / \partial z = 0$ at $z = 0$.

In order to obtain the first term of the series for ζ_1, it is easily found that ζ_{10} satisfies the equation

$$\frac{\partial^2 \zeta_{10}}{\partial z^2} + 2z \frac{\partial \zeta_{10}}{\partial z} = 8\pi^{-\frac{1}{2}} z (2z^2 - 1) \, \mathrm{e}^{-z^2} (\alpha + 2 \sin\theta). \tag{37}$$

The solution satisfying all the conditions is

$$\zeta_{10} = r_3(z) + r_4(z) \sin\theta, \tag{38}$$

where $$r_3(z) = -\alpha[\tfrac{1}{2}(1 - \operatorname{erf} z) + \pi^{-\frac{1}{2}} z (2z^2 + 1) \, \mathrm{e}^{-z^2}],$$

$$r_4(z) = 1 - \operatorname{erf} z - 2\pi^{-\frac{1}{2}} z (2z^2 + 1) \, \mathrm{e}^{-z^2}.$$

The stream function is found by integrating the equation

$$\frac{\partial^2 \psi_{10}}{\partial z^2} = \zeta_{10} + 2z \zeta_{00}, \tag{39}$$

subject to the conditions

$$\psi_{10} = \frac{\partial \psi_{10}}{\partial z} = 0 \quad \text{at} \quad z = 0.$$

This gives

$$\psi_{10} = \frac{\alpha}{4}[z^2(\operatorname{erf} z - 1) + \tfrac{1}{2}\operatorname{erf} z - \pi^{-\frac{1}{2}} z\, \mathrm{e}^{-z^2}] + \tfrac{1}{2}[z^2(1 - \operatorname{erf} z) - \tfrac{1}{2}\operatorname{erf} z + \pi^{-\frac{1}{2}} z(4 - 3\, \mathrm{e}^{-z^2})] \sin\theta. \quad (40)$$

Finally, the function ζ_{11} satisfies the equation

$$\frac{\partial^2 \zeta_{11}}{\partial z^2} + 2z \frac{\partial \zeta_{11}}{\partial z} - 4\zeta_{11} = r_5(z) \cos\theta + r_6(z) \sin 2\theta, \quad (41)$$

where

$$r_5(z) = 4\alpha[-\tfrac{16}{3}\pi^{-\frac{3}{2}} z\, \mathrm{e}^{-z^2} + \pi^{-\frac{1}{2}}(16z^4 + 6z^2 - 1)\, \mathrm{e}^{-z^2} z \operatorname{erf} z + 2\pi^{-1} z^2 (8z^2 - 1)\, \mathrm{e}^{-2z^2} - \tfrac{56}{3}\pi^{-1} z^4\, \mathrm{e}^{-z^2} - 14\pi^{-\frac{1}{2}} z^3\, \mathrm{e}^{-z^2} + (1 - \operatorname{erf} z)^2],$$

$$r_6(z) = 4\pi^{-\frac{1}{2}}\, \mathrm{e}^{-z^2}[z(16z^4 + 6z^2 - 1) \operatorname{erf} z - (6 + \tfrac{16}{3}\pi^{-1}) z + 2\pi^{-\frac{1}{2}} z^2 (8z^2 - 1)\, \mathrm{e}^{-z^2} - 2z^3(1 + \tfrac{28}{3}\pi^{-\frac{1}{2}} z)] - 4 \operatorname{erf} z(1 - \operatorname{erf} z).$$

The solution of (41) is of the form

$$\zeta_{11} = P(z) \cos\theta + Q(z) \sin 2\theta, \quad (42)$$

where $P(z)$ and $Q(z)$ satisfy ordinary differential equations which may be found by substitution of (42) into (41). Solutions for $P(z)$ and $Q(z)$ which satisfy the boundary conditions can probably be found by analytical means, but the solutions would be very complicated and thus, from the known expressions for $r_5(z)$ and $r_6(z)$, they have been found numerically. It may be noted that the solutions are required to vanish as $z \to \infty$ and also to satisfy integral conditions derived from (27). Since there are two conditions for each function $P(z)$ and $Q(z)$, numerical solutions can be found satisfying these conditions. The function ψ_{11} is then found by solving the equation

$$\frac{\partial^2 \psi_{11}}{\partial z^2} = \zeta_{11} + 2z\zeta_{01}, \quad (43)$$

subject to the conditions $\psi_{11} = \partial\psi_{11}/\partial z = 0$ when $z = 0$.

It is found from the numerical solutions that

$$\left.\begin{aligned} P(0) &= 2.78444\alpha, \quad P'(0) = -5.79901\alpha, \\ Q(0) &= 6.5577, \quad Q'(0) = -14.3122, \end{aligned}\right\} \quad (44)$$

where the prime denotes differentiation with regard to z. We thus finally obtain an expression for the vorticity

$$\zeta(z, \theta, \tau) \sim \zeta_{00} + \tau\zeta_{01} + \lambda(\zeta_{10} + \tau\zeta_{11}) \quad (45)$$

which is valid for small τ and large R. It gives sufficient information obtained by analytical means to check the numerical solutions which are obtained by numerical

integration of (24) and (25) subject to the boundary conditions (26) and (27). In particular, we find for the surface vorticity

$$\zeta(0,\theta,\tau) \sim \alpha(2\pi^{-\frac{1}{2}}-\tfrac{1}{2}\lambda)+(4\pi^{-\frac{1}{2}}+\lambda)\sin\theta+(2.7844\lambda-\tfrac{16}{3}\pi^{-\frac{3}{2}})\alpha\tau\cos\theta$$
$$+[6.5577\lambda-4\pi^{-\frac{1}{2}}(1+\tfrac{4}{3}\pi^{-1})]\tau\sin 2\theta. \quad (46)$$

Some further results derived from these solutions will be given subsequently.

4. Numerical methods

We need only briefly describe the methods used to solve numerically (24) and (25) subject to (27) and (28). Nevertheless, this is a very important part of the paper since the main results presented in the following section are based on these numerical solutions. All (25) are of the same form and we need only deal with a typical equation. Thus (25*b*) may be written

$$4\tau\frac{\partial g_n}{\partial\tau} = q_n(z,\tau), \quad (47)$$

where

$$q_n(z,\tau) = \mathrm{e}^{-2\lambda z}\frac{\partial^2 g_n}{\partial z^2}+2z\frac{\partial g_n}{\partial z}+(2-\mathrm{e}^{-2\lambda z}\lambda^2 n^2)g_n+2\tau\,\mathrm{e}^{-2\lambda z}\left[nF_n\frac{\partial G_0}{\partial z}+T_n\right]. \quad (48)$$

Assuming all functions have been determined at time $\tau-\Delta\tau$, we wish to advance the solution to the next time step τ. This is done by a form of the Crank–Nicolson procedure. We integrate both sides of (47) from $\tau-\Delta\tau$ to τ at a given z, performing integration by parts on the integral on the left-hand side, and then replace the resulting integrals by trapezoidal quadrature formulae. This gives the result

$$4(\tau-\tfrac{1}{2}\Delta\tau)[g_n(z,\tau)-g_n(z,\tau-\Delta\tau)] = \tfrac{1}{2}\Delta\tau[q_n(z,\tau)+q_n(z,\tau-\Delta\tau]. \quad (49)$$

We now substitute for q_n in (49) using (48) and then replace derivatives of g_n with respect to z by central differences at the point z. It is then found that (49) is replaced by the equation

$$A_n(z,\tau)g_n(z-\Delta z,\tau)+B_n(z,\tau)g_n(z,\tau)+C_n(z,\tau)g_n(z+\Delta z,\tau)$$
$$= D_n(z,\tau)+4(\tau-\tfrac{1}{2}\Delta\tau)\frac{(\Delta z)^2}{\Delta\tau}g_n(z,\tau-\Delta\tau)+\frac{(\Delta z)^2}{2}q_n(z,\tau-\Delta\tau), \quad (50)$$

where Δz is the grid size in the z-direction. In this equation the terms A_n, B_n and C_n on the left-hand side come from the first three terms on the right-hand side of (48) after expressing the derivatives in central differences; they are easily identifiable. The term $D_n(z,\tau)$ is given by

$$D_n(z,\tau) = (\Delta x)^2\tau\,\mathrm{e}^{-2\lambda z}\left[nF_n(z,\tau)\frac{\partial G_0(z,\tau)}{\partial z}+T_n(z,\tau)\right], \quad (51)$$

which depends on various other functions through its dependence on $T_n(z,\tau)$. However, if we assume this dependence to be held constant at the stage at which (50) are solved for a particular function $g_n(z,\tau)$, these equations define a tridiagonal matrix which must be inverted to find $g_n(z,\tau)$. Similar sets of finite-difference

equations can be formulated corresponding to (25*a*), which yield tridiagonal matrices to be inverted to determine $G_n(z,\tau)$, again assuming the right-hand sides to be held constant as each inversion is made.

The numerical solution procedure is therefore as follows. At a given time τ the solution already obtained at $\tau-\Delta\tau$ for all the functions is used as a starting approximation. One then computes approximations to the functions $g_n(z,\tau)$, $G_n(z,\tau)$ in turn, for $n = 1, 2, \ldots, N$. Each computation is performed by inverting the tridiagonal matrix defined by (50) with $D_n(z,\tau)$ calculated from (51), using the most recently available information, together with the corresponding set of equations for $G_n(z,\tau)$. After each $g_n(z,\tau)$ or $G_n(z,\tau)$ is obtained, the function $f_n(z,\tau)$ or $F_n(z,\tau)$ which corresponds to it is computed by solving the corresponding equation (24) subject to the appropriate initial conditions (26). The method used for this is the stable method given by Dennis & Chang (1969) in which each equation of (24) is factorized into a pair of first-order equations, one of which is integrated in the direction of increasing z and the other in the direction of z decreasing. The utilization of the boundary conditions in order to do this is explained in detail by Dennis & Chang.

In order for this method to be effective, it is necessary for the integral conditions (27) to have been satisfied. It has been explained by Dennis & Chang that only under these circumstances can step-by-step methods be used. The integral conditions are satisfied as follows. For a given function $g_n(z,\tau)$, or likewise for $G_n(z,\tau)$, the set of finite-difference equations (50) is solved to determine values at $z = \Delta z, 2\Delta z, \ldots, z_M-\Delta z$, where z_M is the value of z at which the conditions $g_n(z_M,\tau) = G_n(z_M,\tau) = 0$ are assumed. The solution procedures require a knowledge of $g_n(0,\tau)$ and $G_n(0,\tau)$. The most recent approximations which have been obtained, say $g_n^{(m)}(0,\tau)$ and $G_n^{(m)}(0,\tau)$, are used for these values. Then, after a solution has been obtained for a given $g_n(z,\tau)$ or $G_n(z,\tau)$, the appropriate integral condition (27) is satisfied by writing the integral as a quadrature formula and then determining a new estimate of $g_n(0,\tau)$ or $G_n(0,\tau)$ from the new calculated set of values of $g_n(z,\tau)$ or $G_n(z,\tau)$ for $z \neq 0$ to satisfy this quadrature formula. This step is carried out immediately after (50) or its counterpart is solved, completing the approximation to $g_n(z,\tau)$ or $G_n(z,\tau)$ for all z in $0 \leqslant z \leqslant z_M$.

The whole iterative procedure is carried out until the difference between two successive iterates of all functions lies within certain limits. For each τ the condition for $g_n(z,\tau)$ was taken as

$$|g_n^{(m+1)}(z,\tau)-g_n^{(m)}(z,\tau)| < 10^{-6} \tag{52}$$

for $n = 1, \ldots, N$ and $0 \leqslant z \leqslant z_M$ with a similar condition on $G_n(z,\tau)$. When (52) is satisfied, all other functions have converged to limits to high accuracy.

The solution at $\tau = 0$ is known from (30) and (31). The variation of vorticity with time is large initially and a quite small time step $\Delta\tau$ is necessary. Thus $\Delta\tau = 10^{-4}$ was taken for the first 10 time steps. It was then increased to $\Delta\tau = 10^{-3}$ for the next 10 steps and then to $\Delta\tau = 10^{-2}$ for the next 10. Finally $\Delta\tau = 0.025$ was taken for the rest of the solution. The grid size in the z-direction was taken as $\Delta z = 0.05$ at the start of the integrations and then increased to $\Delta z = 0.1$ at $\tau = 1.5$. The values of grid sizes were to some extent chosen to be comparable with those used by Collins & Dennis (1973*b*), since these were found to be satisfactory and were checked carefully. A few comparable checks of comparing results on different grids were made at one or two values of τ during the present calculations. Moreover, the solutions obtained by fully numerical means are compared with the results obtained using expansions in powers of τ; these comparisons indicate that the solutions are quite accurate.

As in the case of $\alpha = 0$ considered by Collins & Dennis (1973*b*), very few terms of

the series (8) are required at the start of the integrations and more terms are gradually added as τ increases. In fact, the maximum value of n is increased by unity every time a term preceding it in the series attains an absolute value of 10^{-4} for any value of z in the range $0 \leqslant z \leqslant z_M$. Finally we may note that the numerical method described may be used to continue the solution for increasing τ in terms of the original physical coordinate ξ when the boundary layer thickens. The same methods may be used to integrate (9) and (20) subject to the boundary conditions in terms of these coordinates. However in the present paper only cases for which $R \geqslant 200$ are presented and it is possible to work in terms of the boundary-layer coordinate z over the entire range of τ considered. The maximum value of z was $z_M = 8$.

5. Results and comparisons

In this section we shall present results obtained for two Reynolds numbers, $R = 200$ and 500, at two rotation speeds $\alpha = \frac{1}{2}$, 1. These will be given in terms of variation of streamline patterns and surface vorticity with time. Further results for the lift and drag coefficients and some other properties of the flow are given at higher Reynolds numbers. The results were computed by starting the solution with two terms in each of (8a) and (8b) and continuing the integrations until τ reached 12.0, by which time 33 terms (corresponding to $N = 15$) were used in each series. Although the case of relatively large values of α is of considerable interest in view of previous theoretical work, it is more difficult to maintain accurate results as α increases and so only results for small α are presented.

We can obtain simple formulae for the lift and drag results at small values of τ by making use of formulae which may be found in order to calculate these same quantities numerically from the numerical solutions. If L and D are the lift and drag on the cylinder, the lift, drag and moment coefficients are defined by

$$C_L = \frac{L}{\rho U^2 a}, \quad C_D = \frac{D}{\rho U^2 a}, \quad C_M = \frac{M}{4\pi\mu a^2 \omega_0}, \tag{53}$$

where M is the frictional moment. The lift and drag coefficients each consist of components due to the friction forces and the pressure. If we integrate these forces over the surface of the cylinder it is found that

$$C_D = \frac{2}{R}\int_0^{2\pi} \zeta_0 \sin\theta \, \mathrm{d}\theta - \frac{1}{2}\int_0^{2\pi} p_0^* \cos\theta \, \mathrm{d}\theta, \tag{54a}$$

$$C_L = -\frac{2}{R}\int_0^{2\pi} \zeta_0 \cos\theta \, \mathrm{d}\theta - \frac{1}{2}\int_0^{2\pi} p_0^* \sin\theta \, \mathrm{d}\theta, \tag{54b}$$

where the first integral in each gives the coefficient due to friction and the second that due to the pressure. The subscript denotes a value at the surface $\xi = 0$ and p_0^* is the pressure coefficient

$$p_0^* = \frac{p_0(\theta,\tau) - p_0(\pi,\tau)}{\frac{1}{2}\rho U^2}. \tag{55}$$

We can evaluate the integrals in (54) using the series for $\zeta(\xi,\theta,\tau)$. The first integral in each of (54) is evaluated directly while the second of each is evaluated by integration by parts and then using the result

$$\frac{\partial p_0^*}{\partial\theta} = -\frac{4}{R}\left(\frac{\partial\zeta}{\partial\xi}\right)_{\xi=0}. \tag{56}$$

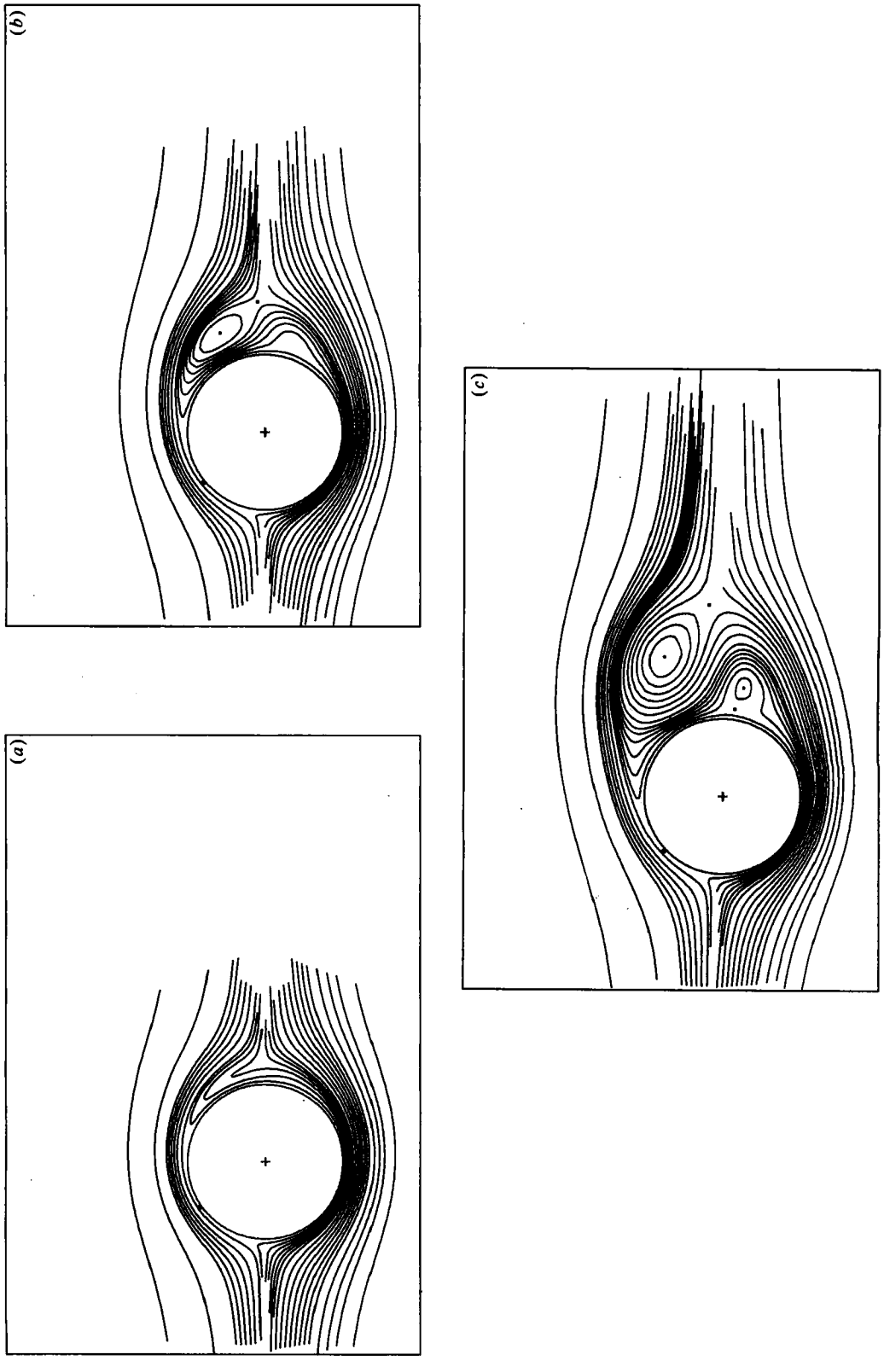

FIGURE 1 (*a*, *b*, *c*). For caption see page 463.

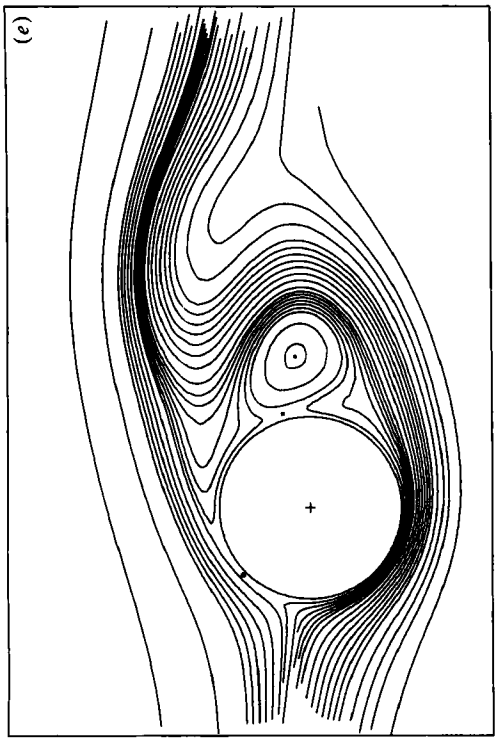

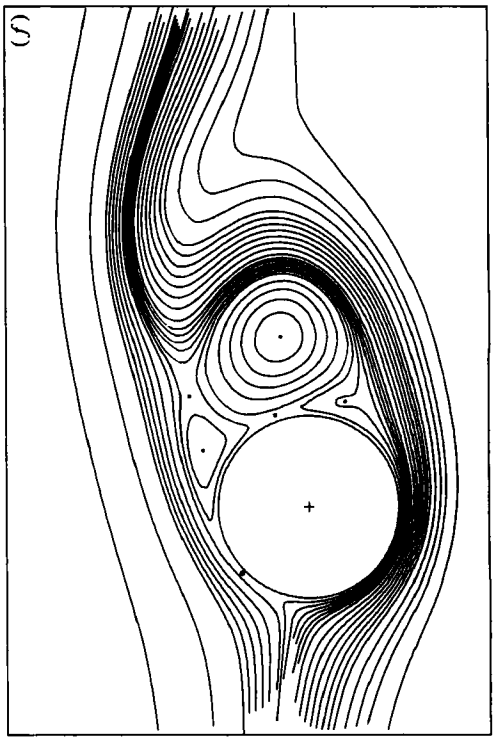

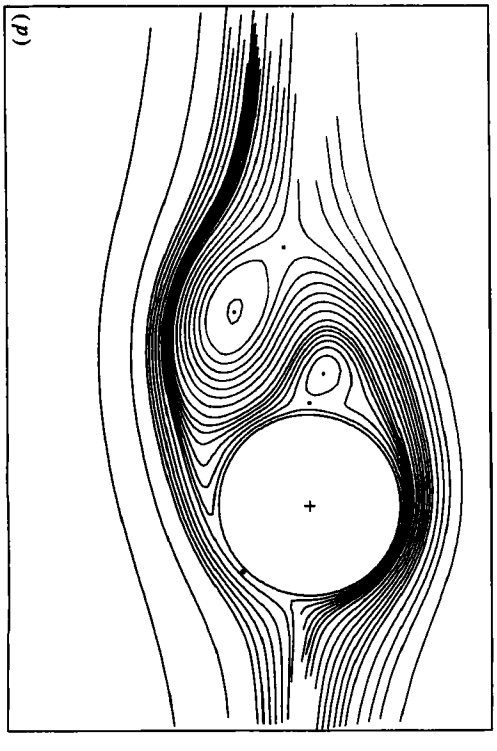

FIGURE 1 (*d*, *e*, *f*). For caption see facing page.

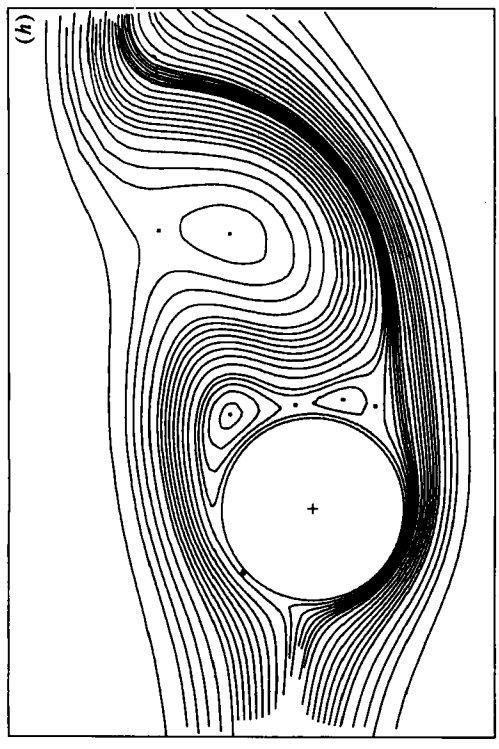

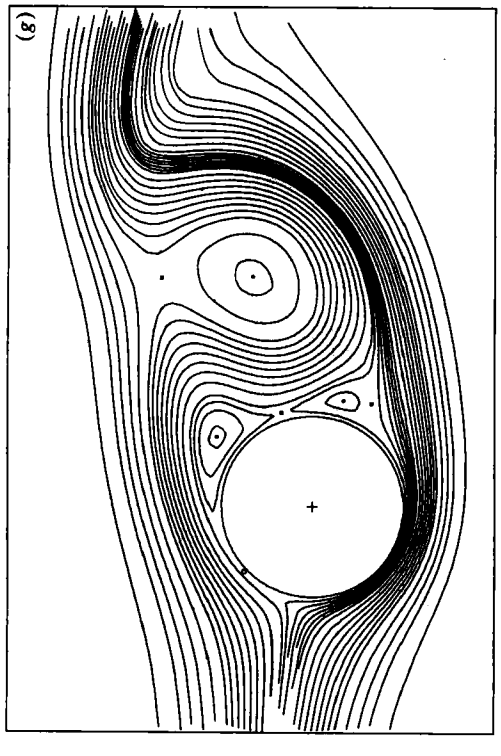

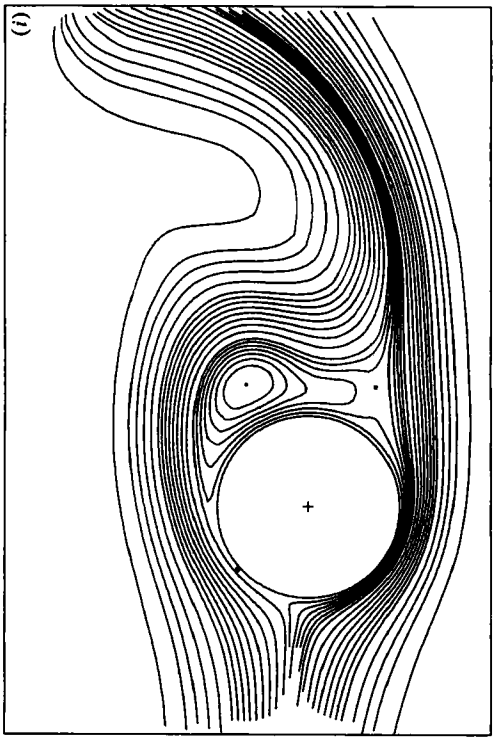

FIGURE 1. Instantaneous streamlines of the flow for $R = 200$, $\alpha = \frac{1}{4}$ at various times: (*a*) $\tau = 1.0$; (*b*) 2.0; (*c*) 4.0; (*d*) 5.0; (*e*) 7.0; (*f*) 8.0; (*g*) 10.0; (*h*) 11.0; (*i*) 12.0. In each case: ○, front stagnation point; ●, vortex centre; ■, closure point of vortex. In (*g*)–(*i*) the streamlines from top to bottom of each diagram at the front of the cylinder correspond to the values $\psi = 1.0, 0.8, 0.7, 0.6, 0.5, 0.4, 0.35, 0.3, 0.25, 0.2, 0.15, 0.1, 0.05, 0, -0.02, -0.04, -0.06, -0.08, -0.1, -0.12, -0.15, -0.2, -0.25, -0.3, -0.35, -0.4, -0.45, -0.5, -0.6, -0.7, -0.8, -1.0$; in (*a*)–(*f*) the streamlines for $\psi = 0.8, 0.7, 0.6, 0.4, 0.35, 0.3$ are omitted.

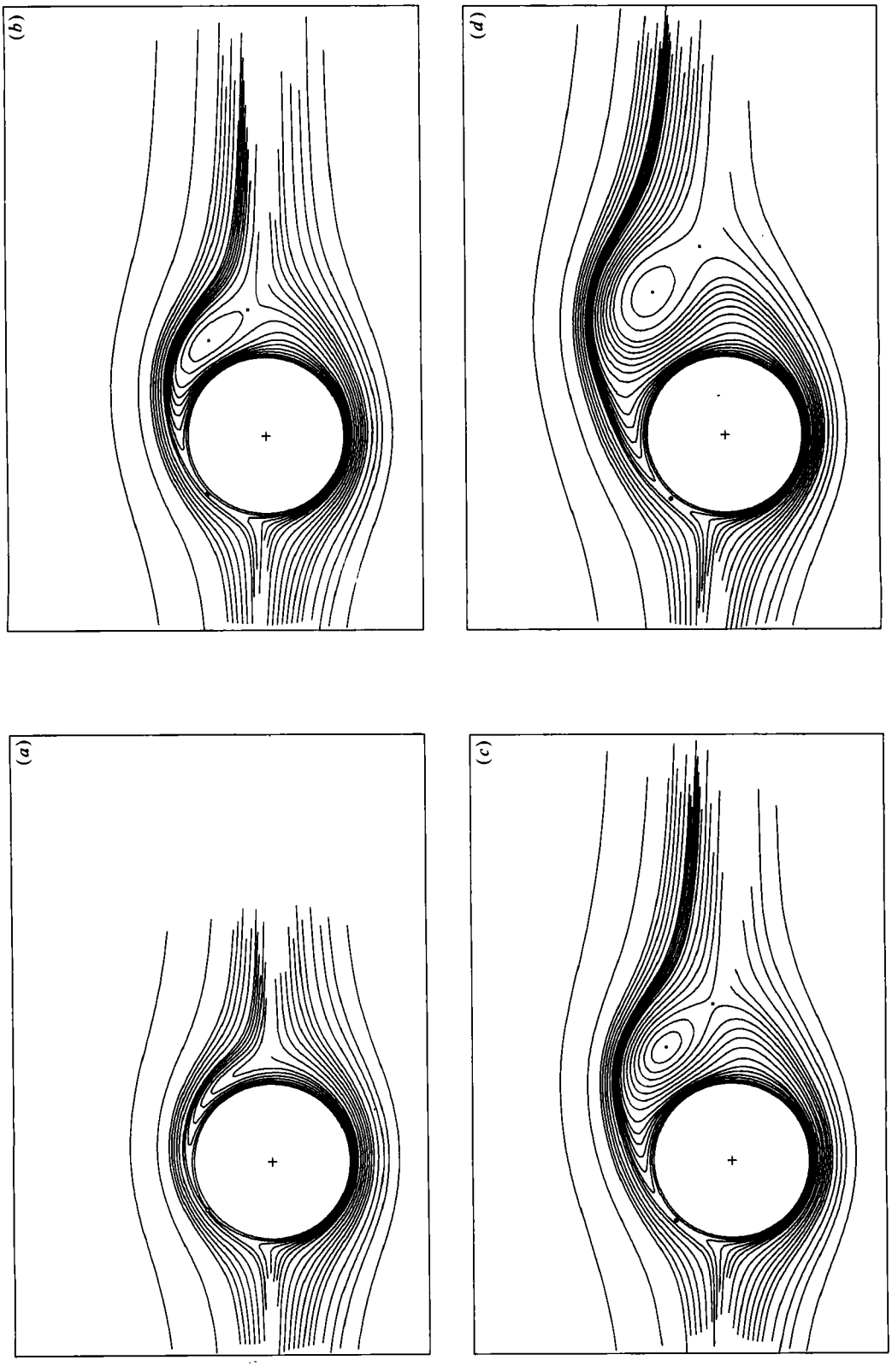

FIGURE 2 (*a*, *b*, *c*, *d*). For caption see page 467.

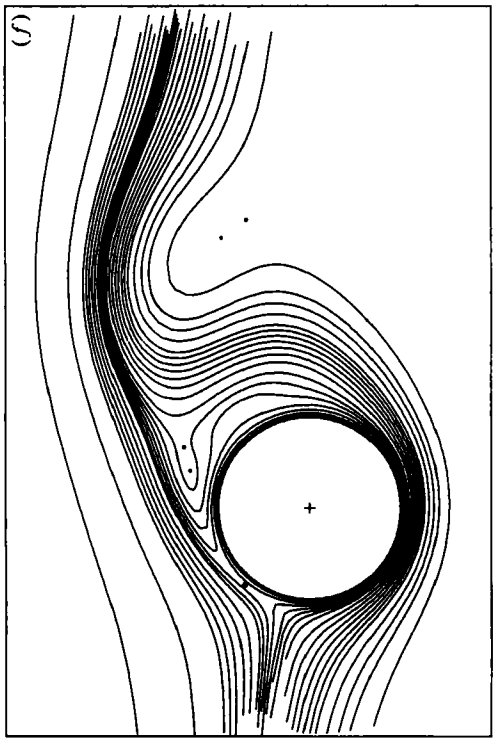

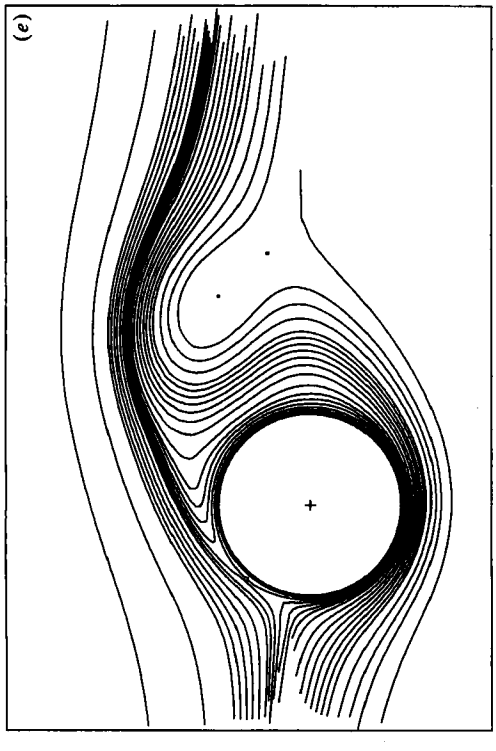

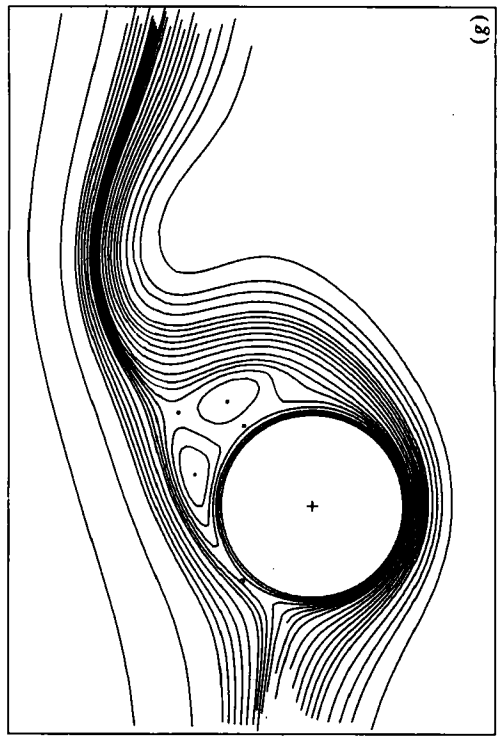

FIGURE 2 (*e*, *f*, *g*). For caption see page 467.

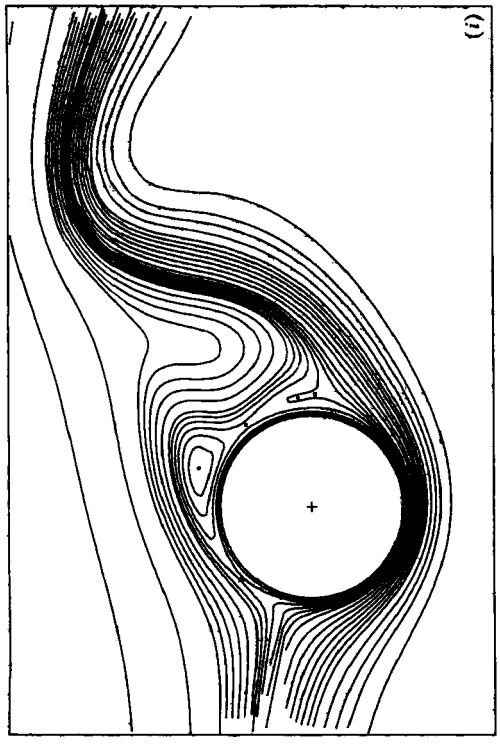

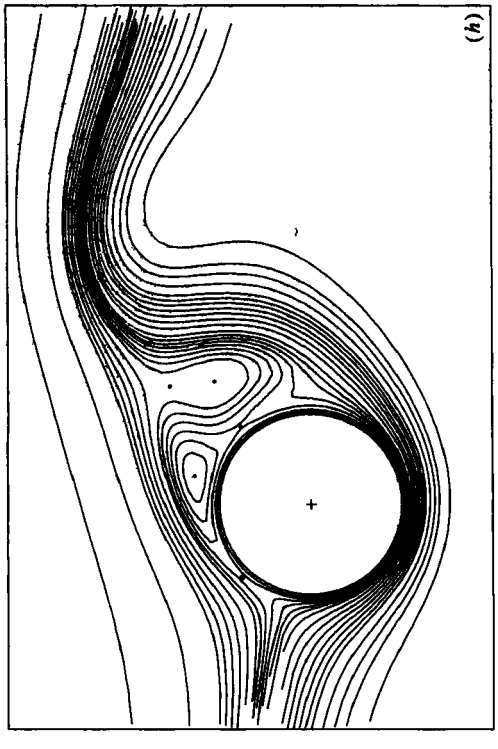

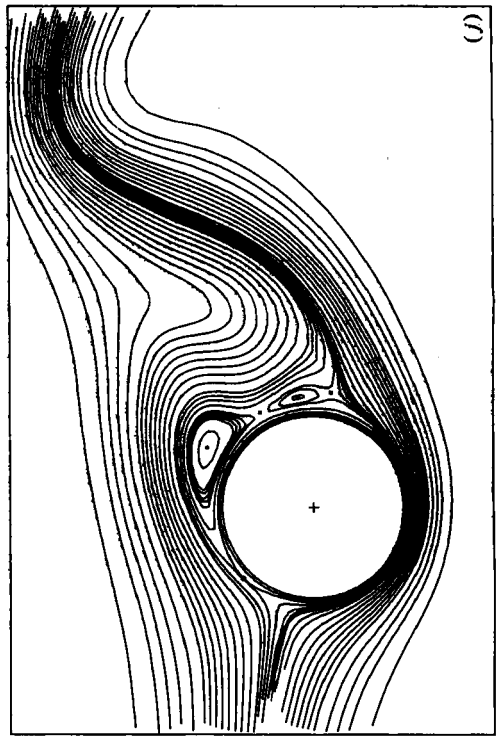

FIGURE 2 (*h*, *i*, *j*). For caption see facing page.

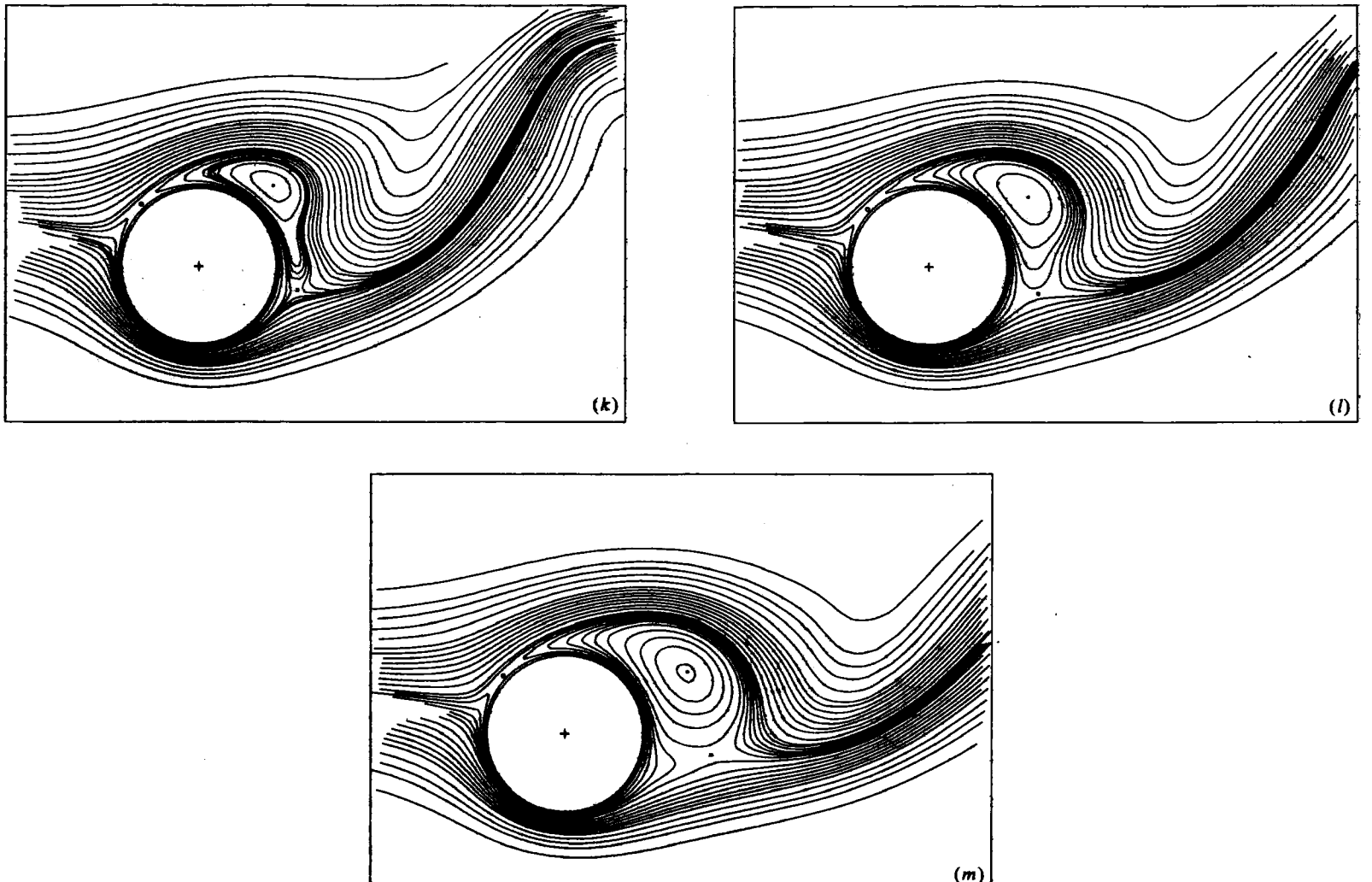

FIGURE 2. Instantaneous streamlines of the flow for $R = 200$, $\alpha = 1$ at various times: (*a*) $\tau = 1.0$; (*b*) 2.0; (*c*) 3.0; (*d*) 4.0; (*e*) 5.0; (*f*) 6.0; (*g*) 6.5; (*h*) 7.0; (*i*) 8.0; (*j*) 9.0; (*k*) 10.0; (*l*) 11.0; (*m*) 12.0. The streamlines in (*a*)–(*i*) correspond to the values of ψ in (*a*)–(*f*) of figure 1 and those in (*l*) and (*m*) correspond to the values of ψ in (*g*)–(*i*) of figure 1. In (*j*) and (*k*) an extra streamline $\psi = -0.09$ has been added between $\psi = -0.1$ and -0.08. The notation for special points is as in figure 1.

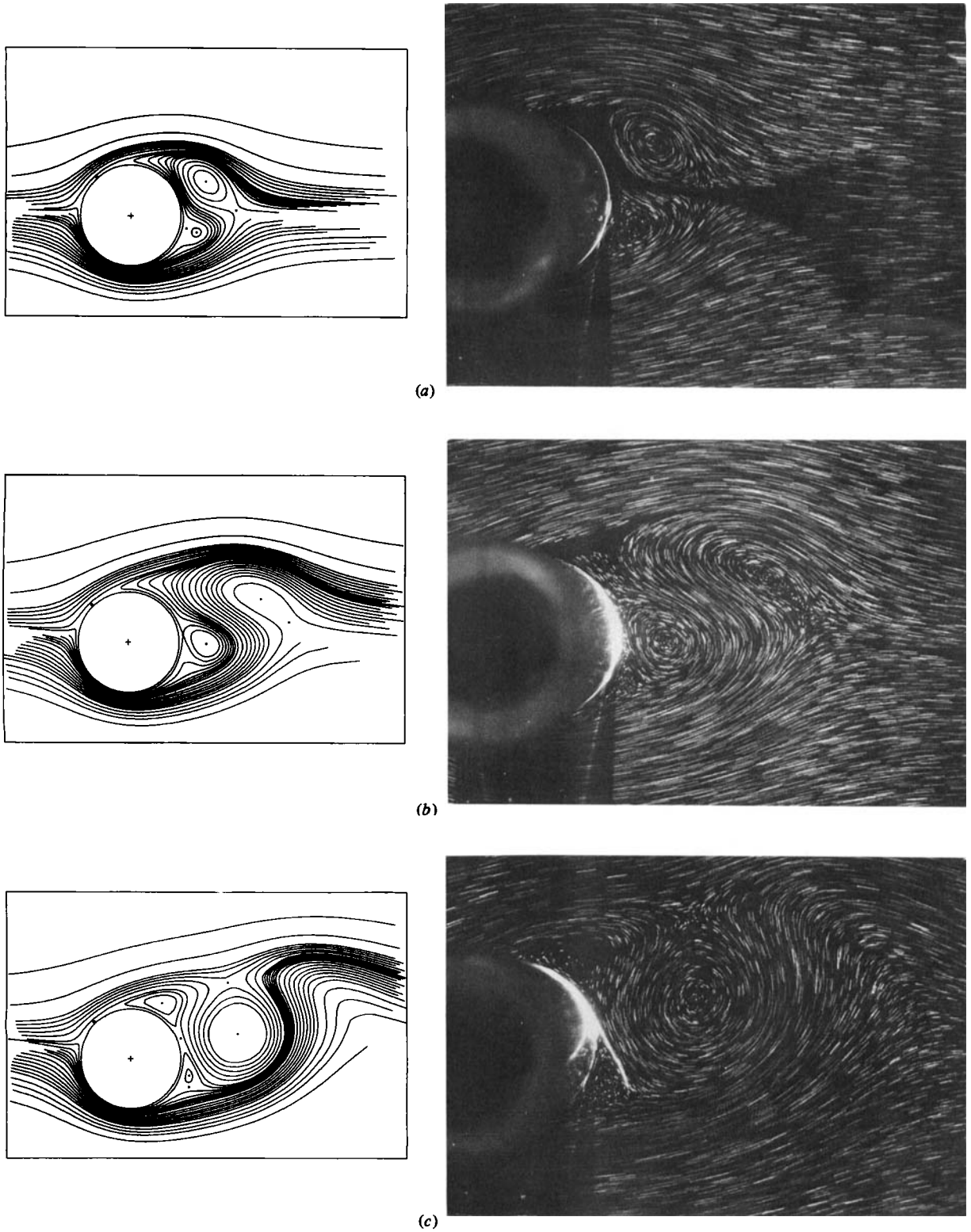

FIGURE 3. Comparison of calculated and experimental instantaneous streamlines for $R = 200$; $\alpha = \frac{1}{2}$: (*a*) $\tau = 3.0$; (*b*) 6.0; (*c*) 9.0.

Thus we obtain

$$C_D = \frac{2\pi}{R}\left[g_1(0,\tau) - \left(\frac{\partial g_1}{\partial \xi}\right)_{\xi=0}\right], \quad C_L = -\frac{2\pi}{R}\left[G_1(0,\tau) - \left(\frac{\partial G_1}{\partial \xi}\right)_{\xi=0}\right]. \quad (57a, b)$$

The numerical work of the present paper has been carried out in terms of boundary-layer coordinates whereas the functions in (57) are those defined in (8*b*). We must therefore substitute the boundary-layer variables defined in (22) and (23) in evaluating (57); the modifications of (57) are obvious. It may be noted that the lift and drag coefficients depend only on g_1, G_1 and their derivatives. These functions are determined fairly accurately in the numerical process, which leads to accurate results for C_D and C_L. We may also obtain exact expressions for C_D and C_L valid at small values of τ by making use of (46). It may be shown that the expression for p_0^* found from (56) using (46) is

$$p_0^* = -\frac{4}{R\lambda^2}\left[4\pi^{-\frac{1}{2}}\lambda(1+\cos\theta) + \tfrac{1}{2}\tau(8-\lambda q_2)(1-\cos 2\theta) - q_1\lambda\tau\alpha\sin\theta\right], \quad (58)$$

where $q_1 = 5.79901$, $q_2 = 14.3122$. We can substitute directly from (46) and (58) into (54) to obtain expressions for the lift and drag coefficients which are valid for small τ. It is found that

$$C_D \sim \frac{\pi}{(2R\tau)^{\frac{1}{2}}}\left(\frac{8}{\pi^{\frac{1}{2}}} + 2\left(\frac{2\tau}{R}\right)^{\frac{1}{2}}\right); \quad (59)$$

$$C_L \sim -\alpha[(1.4498\pi - \tfrac{4}{3}\pi^{-\frac{1}{2}})\lambda + 0.6961\pi\lambda^2]. \quad (60)$$

From the same details of the initial solution it is found that the frictional-moment coefficient obtained by integration of the moment of the frictional shear stress on the cylinder around it is given by

$$C_M \sim \tfrac{1}{2}\lambda^{-1}(2\pi^{-\frac{1}{2}} - \tfrac{1}{2}\lambda). \quad (61)$$

The expressions (59)–(61) can all be used to check the results of the numerical integrations at small values of τ; results of these checks will be given shortly.

We shall now present the results of calculations for the cases $R = 200$, $\alpha = \frac{1}{2}$ and $\alpha = 1$; these may be compared with the recent experimental results of Coutanceau & Ménard (1985) for the same case. The experimental set-up is described in the paper cited. The start of the motion is virtually instantaneous and the development of the flow is visualized by a moving camera which accompanies the cylinder in its translational motion, in effect simulating exactly the translating frame of reference without rotation used in the present study. In figures 1 and 2 we give the streamlines for the developing flow at various values of τ for the respective cases $\alpha = \frac{1}{2}$, 1. The corresponding flow visualizations of Coutanceau & Ménard (1985) are exhibited in their figures 6 and 9; for continuity of their study with the present one we give, in figure 3, some selected comparisons for one case. It may be seen that the calculations are virtually identical with the flow visualizations. Moreover some detailed quantitative comparisons can be made which indicate the precision of the agreement between theory and experiment.

Coutanceau & Ménard have made a detailed study of the motion of the centres of the vortices which form at the rear of the cylinder and ultimately detach into the wake during the motion. They have also studied the motion of the stagnation points, or saddle points, which form the points of closure of the vortices after their formation. Telionis (1981) indicates that these points are of some theoretical interest in studying

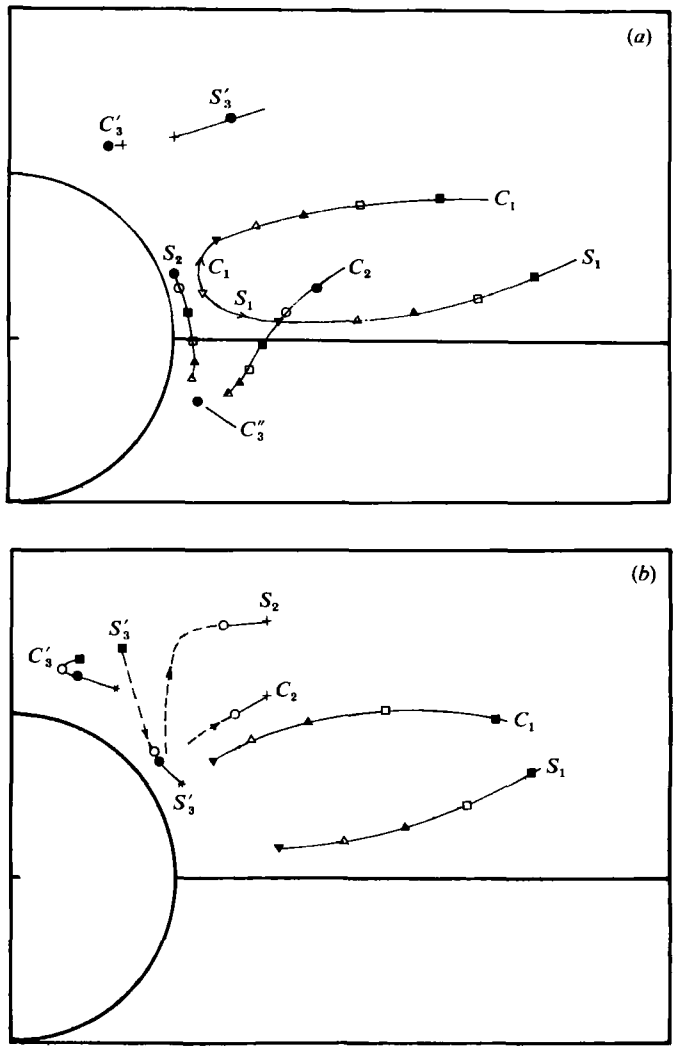

FIGURE 4. Paths of the centres C_i and closure points S_i of each of the first three vortices ($i = 1, 2, 3$) for $R = 200$ and (*a*) $\alpha = \frac{1}{2}$; (*b*) 1. The notation for C_i and S_i is that of Coutanceau & Ménard (1985). The times correspond to: ▽, $\tau = 1$; ▼, 2; △, 3; ▲, 4; □, 5; ■, 6; ○, 7; +, 7.5; ●, 8; *, 9.

the nature of the flow at the onset of separation. In the present numerical study the motion of both the centres and the closure points of the vortices can clearly be seen in figures 1 and 2. After the vortices detach from the cylinder and move downstream they eventually open up and the closure points disappear. This phenomenon has been observed by Coutanceau & Ménard and is also clearly seen in figures 1 and 2.

In figures 4(*a*, *b*) are shown, for the respective cases $\alpha = \frac{1}{2}$ and 1, the paths of the centres C_1, C_2 and C_3 of the vortices which have formed, in that order, from the start of the motion to the time at which the calculations were terminated. The paths of the closure points S_1, S_2 and S_3 which respectively correspond to these vortices are also shown. The time of termination of the calculations was $\tau = 12.0$ both for $\alpha = \frac{1}{2}$ and 1. The results may be compared with the experimental observations of Coutanceau & Ménard (1985, figures 13*a* and *b*) where it will be found that the comparisons are

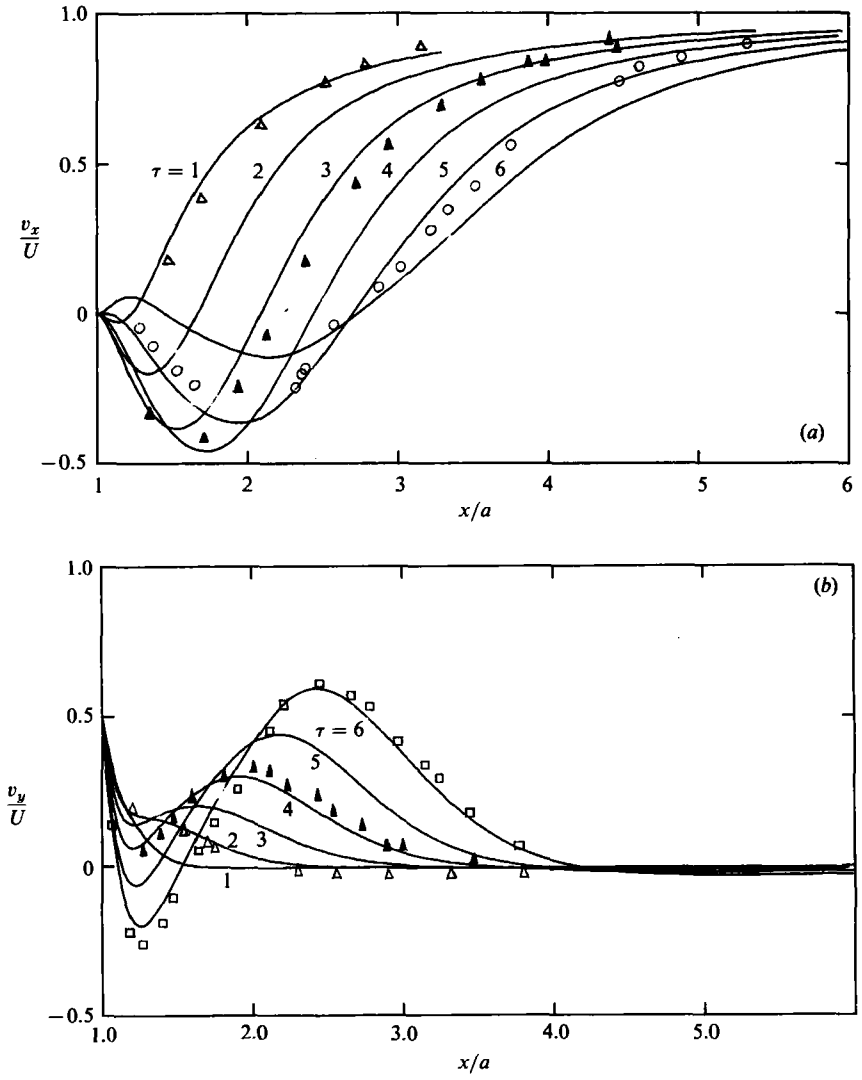

FIGURE 5. Time development of velocity profiles and comparison with the experimental results of Coutanceau & Ménard (1985) for $R = 200, \alpha = \frac{1}{2}$. (*a*) x-component of velocity on $\theta = 0$. Experimental values: △, $\tau = 1.0$; ▲, 3.0; ○, 5.0. Theoretical; curves ——. (*b*) y-component of velocity on $\theta = 0$. Experimental values: △, $\tau = 2.0$; ▲, 4.0; □, 6.0. Theoretical curves ——.

virtually identical in every respect. In the case of $\alpha = \frac{1}{2}$ (figure 4*a*) the vortex C_1 forms first above the x-axis and then C_2 forms later, below the x-axis. After a while C_1 detaches and moves downstream. The associated stagnation (closure) point S_1 exists for a while and then vanishes somewhere just after $\tau = 6$ as the vortex opens up. After C_1 has detached, the vortex C_2 moves up and grows (see figure 1*e*). It eventually detaches and passes downstream also but, before it does so, we find precisely the same almost discontinuous change of position of the closure point S_2 observed in the experiments. This sudden change in the position of S_2 occurs between $\tau = 7$ and 8, exactly as in the experiments. After C_2 has detached, two vortices appear almost simultaneously, one above the x-axis and the other below. We can denote them by

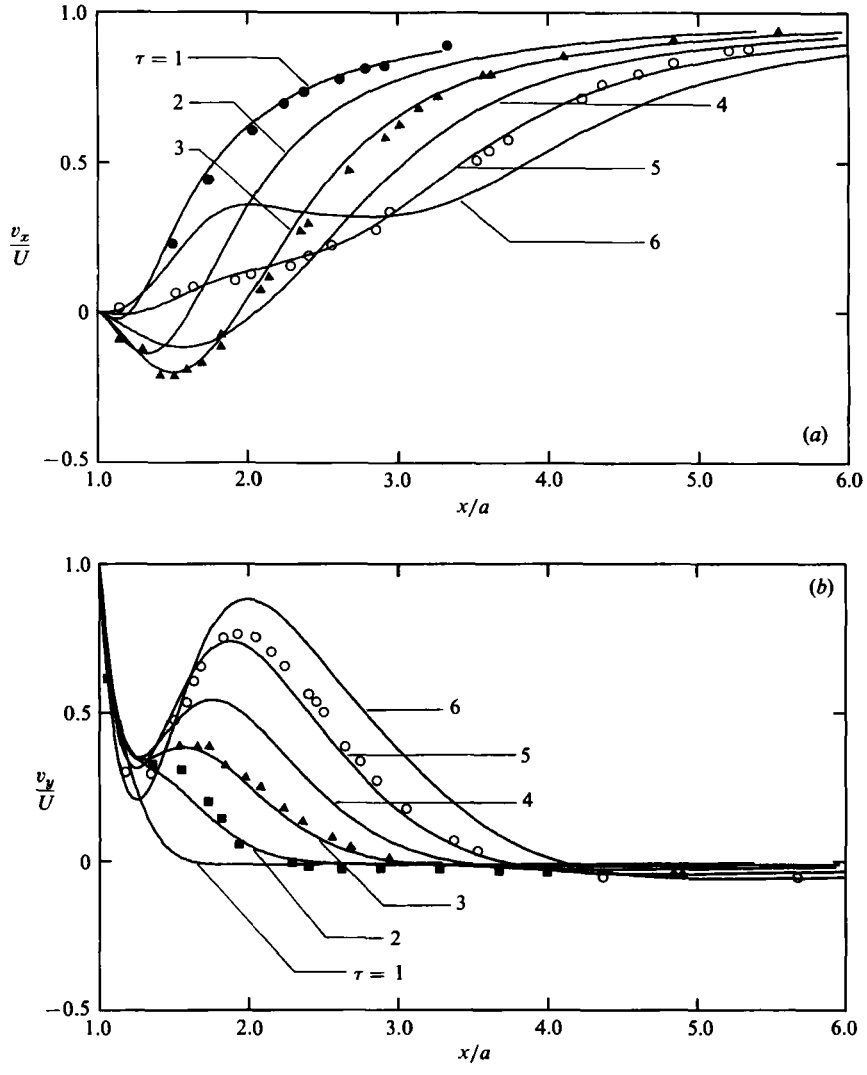

FIGURE 6. Time development of velocity profiles and comparison with the experimental results of Coutanceau & Ménard (1985) for $R = 200, \alpha = 1$. (*a*) x-component of velocity on $\theta = 0$. Experimental values: ●, $\tau = 1.0$; ▲, 3.0; ○, 5.0. Theoretical curves ——. (*b*) y-component of velocity on $\theta = 0$. Experimental values: ■, $\tau = 2.0$; ▲, 3.0; ○, 5.0. Theoretical curves ——.

C_3' and C_3''. They have formed in figure 3(*c*) and gradually grow (see figure 1(*g*), and figure 6(*k*) of Coutanceau & Ménard). At this stage C_2 has passed further downstream and become quite large. Eventually C_3' and C_3'' coalesce to form C_3; this is shown in figure 1(*i*), and figure 6(*m*) of Coutanceau & Ménard. The same sudden change of the position of the closure point S_2 noted in the case $\alpha = \frac{1}{2}$ occurs also in the case $\alpha = 1$ and is shown fairly clearly in figure 4(*b*).

The somewhat different behaviour in the cases $\alpha = \frac{1}{2}$ and 1 noted in the experiments of Coutanceau & Ménard is followed closely in the numerical results. In particular, we observe that the increase in the rate of rotation inhibits the formation of the lower vortex (below the x-axis). Then at $\tau > 6$ the new sequence of phenomena which occur in the vortex formation in this case is again identical in the theoretical and

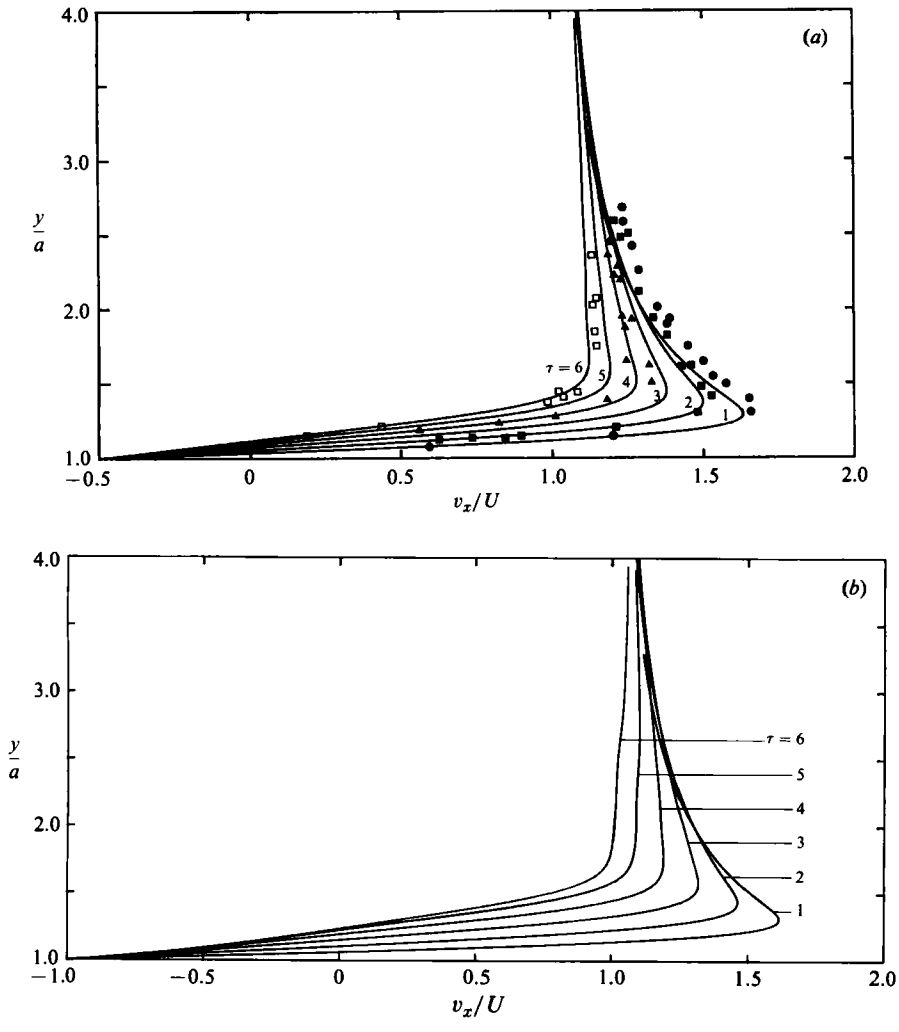

FIGURE 7. The time development of the x-component of velocity on $\theta = 90°$ when $R = 200$ for (a) $\alpha = \frac{1}{2}$; (b) 1. Experimental results of Coutanceau & Ménard (1985): ●, $\tau = 1.0$; ■, 2.0; ▲, 4.0; □, 6.0. Theoretical curves ——.

experimental results. The tendency for the lower vortex not to form increases with increasing α. This is clearly shown in Coutanceau & Ménard's experiments. In fact at $\alpha = 2.07$ the vortex below the x-axis with centre C_2 does not form at all in the time range $\tau = 0$–9 of the observations and for $\alpha = 3.25$ no other vortex than the first, with centre C_1, appears. The numerical calculations become more difficult as α increases and we have restricted the present study to $\alpha \leqslant 1$.

As a further check on the consistency of the experimental and calculated results for $R = 200$, the velocity profiles are compared in several locations. Figures 5 (a, b) show the evolution with time of the x- and y-components of velocity, v_x and v_y respectively, on the axis $\theta = 0$ to the rear of the cylinder for the case $\alpha = \frac{1}{2}$ up to $\tau = 6$, and figures 6 (a, b) give the corresponding results for $\alpha = 1$. They may be compared with figures 17 (a, b) and 18 (a, b) of Coutanceau & Ménard (1985) which indicate a good measure of quantitative agreement. Some representative points taken from the

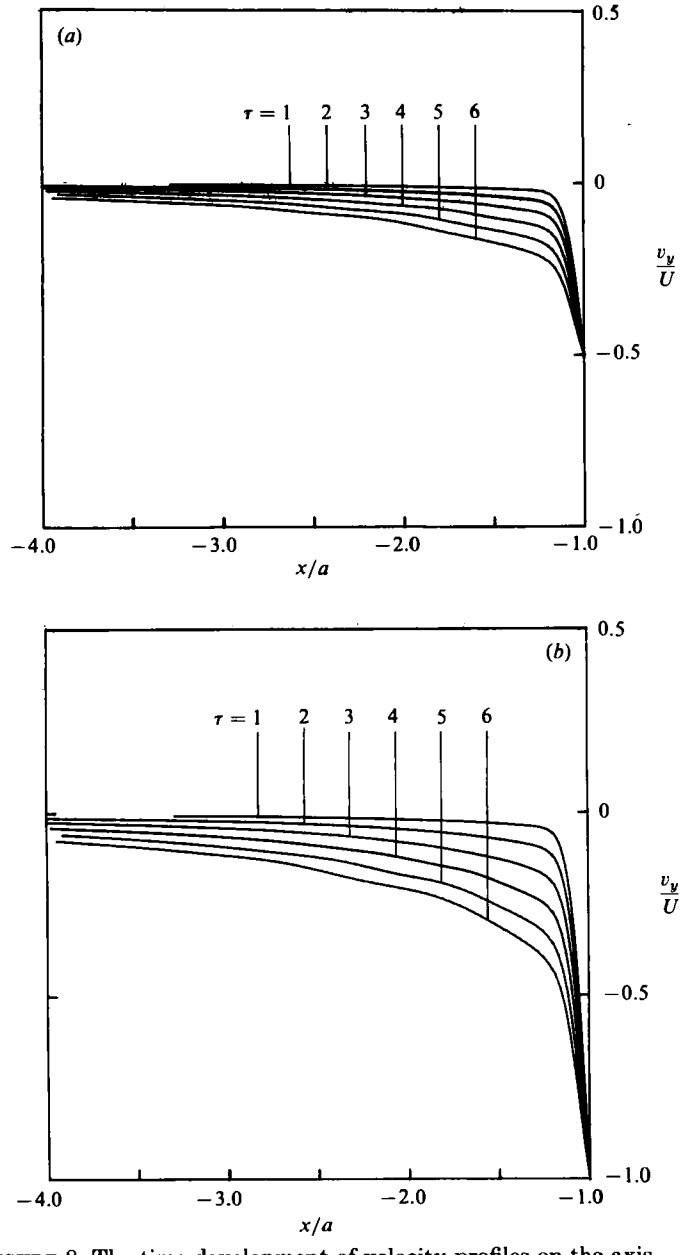

FIGURE 8. The time development of velocity profiles on the axis $\theta = \pi$ for the case $R = 200$: (*a*) $\alpha = \frac{1}{2}$; (*b*) 1.

experimental study are shown in figures 5 and 6 to illustrate the degree of the quantitative comparison. In figure 7 (*a*) we compare the x-component of velocity on the axis $\theta = \frac{1}{2}\pi$ with Coutanceau & Ménard's experimental results for $\alpha = \frac{1}{2}$ (given in their figure 19). There is a certain amount of scatter in the experimental results, particularly at the larger distances from the cylinder. Nevertheless the overall trends of the calculated and experimental results coincide quite well, and extremely well near the cylinder. The corresponding calculated results for $\alpha = 1$ are given in figure 7 (*b*). Finally, in figures 8 (*a*, *b*) some results are given for the y-component of velocity on

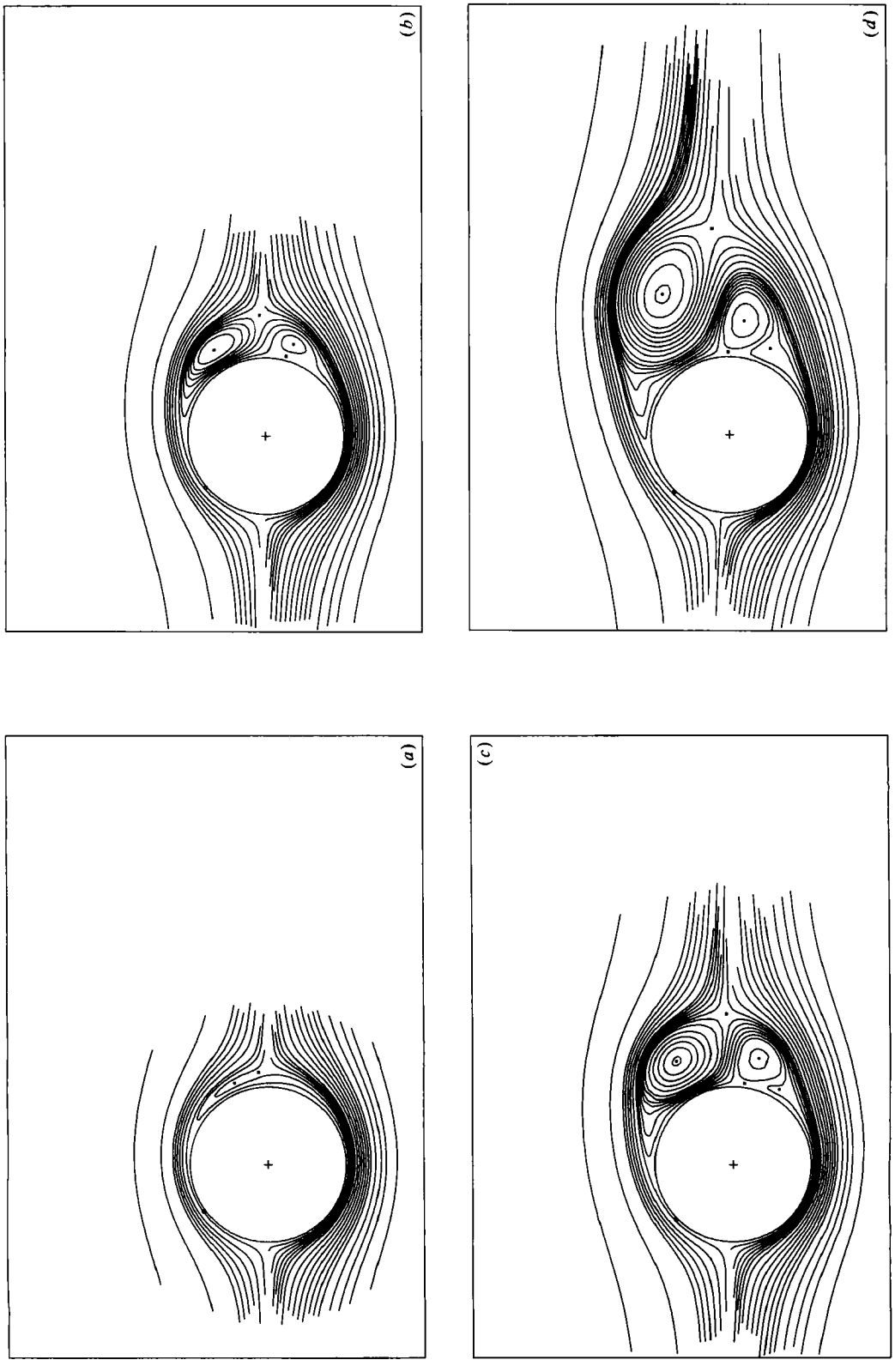

FIGURE 9 (*a*, *b*, *c*, *d*). For caption see page 477.

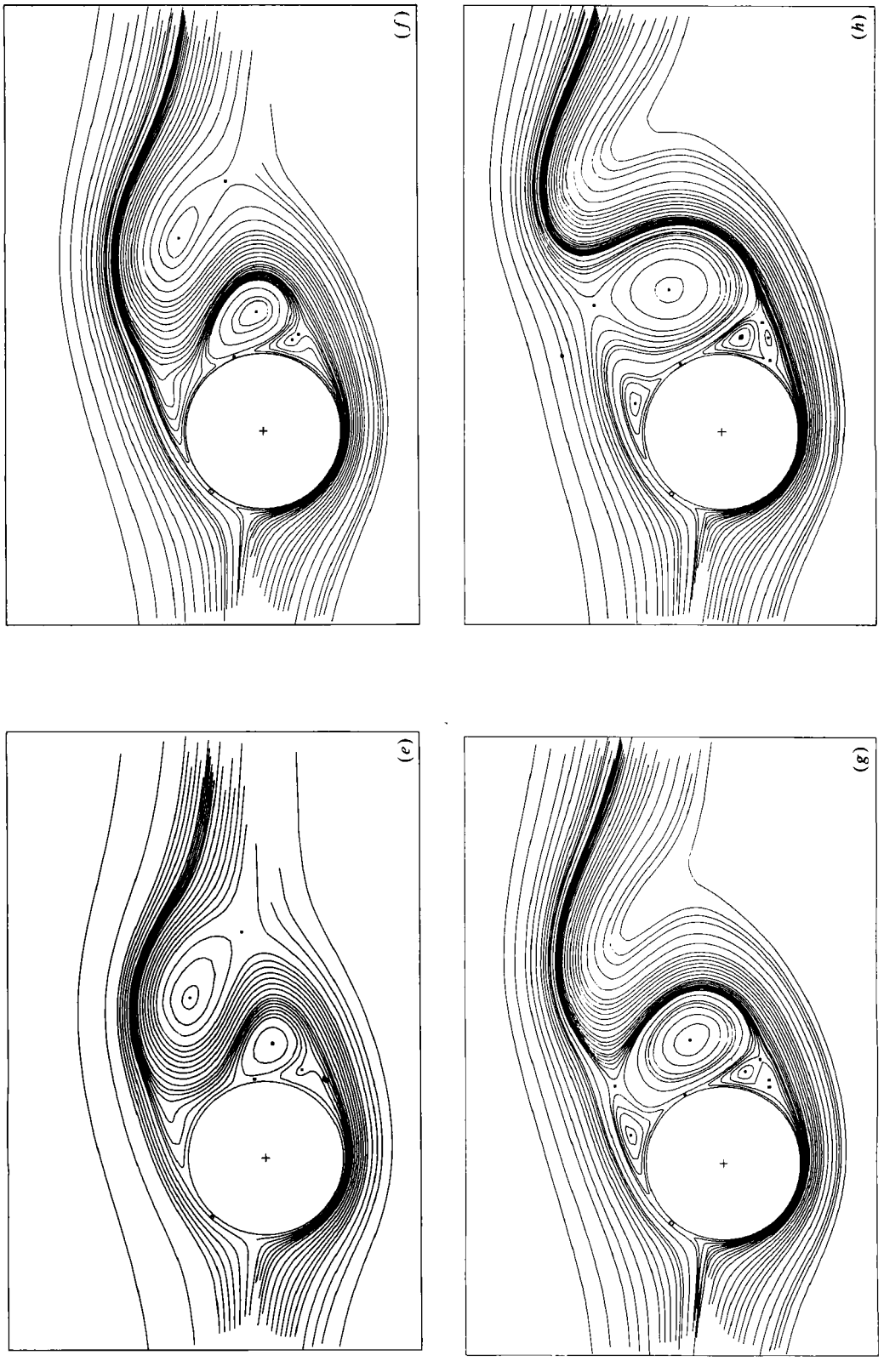

FIGURE 9 (*e*, *f*, *g*, *h*). For caption see facing page.

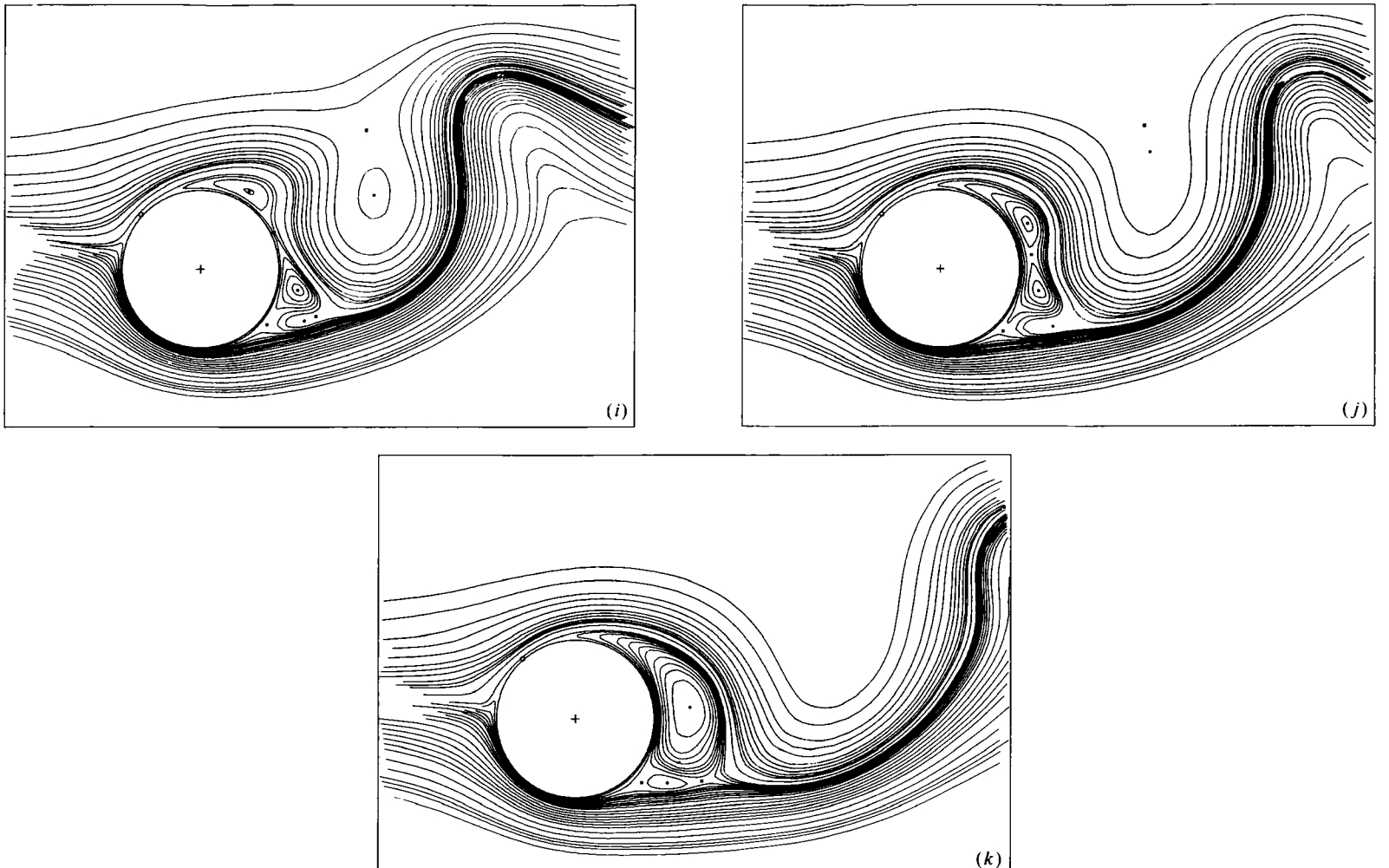

FIGURE 9. Instantaneous streamlines of the flow for $R = 500$, $\alpha = \frac{1}{2}$ at various times: (*a*) $\tau = 1.0$; (*b*) 2.0; (*c*) 3.0; (*d*) 5.0; (*e*) 6.0; (*f*) 7.0; (*g*) 8.0; (*h*) 9.0; (*i*) 10.0; (*j*) 11.0; (*k*) 12.0. In (*f*)–(*k*) the streamlines from top to bottom at the front of the cylinder correspond to $\psi = 1.0, 0.8, 0.6, 0.5, 0.4, 0.3, 0.25, 0.2, 0.15, 0.12, 0.1, 0.05, 0, -0.01, -0.02, -0.03, -0.04, -0.05, -0.06, -0.08, -0.1, -0.12, -0.15, -0.2, -0.25, -0.3, -0.35, -0.4, -0.45, -0.5, -0.6, -0.7, -0.8, -0.85, -0.9, -1.0$; in (*a*)–(*e*) the streamlines for $\psi = 0.8, 0.6, 0.4, 0.3, 0.12, -0.01, -0.03, -0.05, -0.85, -0.9$ are omitted. The notation for special points is as in figure 1.

the axis $\theta = 180°$ when $\alpha = \frac{1}{2}, 1$. They show the customary type of boundary-layer decay to a zero y-component of velocity outside the boundary layer with a rather slower decay and a thickening of the boundary layer as τ increases.

We shall now present some results for the case $R = 500$. No experimental observations are given for this case by Coutanceau & Ménard (1985) but some brief comparisons of their observations of instantaneous streamlines of the flow for $R = 500$, $\alpha = \frac{1}{2}$ and 1 with the present calculations are noted by Badr *et al.* (1985). The calculated results given now are also for the two small rotation rates $\alpha = \frac{1}{2}$ and 1. The streamlines of the developing flow in these two cases are shown respectively in figures 9 and 10 for values of τ up to 12.0, at which time the calculations were terminated. In both cases a separated region forms first at the surface of the cylinder above the x-axis ($\frac{1}{4}\pi < \theta < \frac{1}{2}\pi$) as in the case of $R = 200$. In the case $\alpha = \frac{1}{2}$ a second vortex forms in the region just below the x-axis soon after the formation of the first. They both grow until eventually the first detaches from the cylinder and passes downstream. The second continues to grow and ultimately detaches from the cylinder after the formation of two new vortices respectively above and below the x-axis near the cylinder (figure 9*g*). These subsequently coalesce and then (figure 9*k*) a new vortex is formed below the x-axis, after which the calculations were terminated.

In the case $\alpha = 1$ the flow develops somewhat differently because of the higher rate of rotation. The main difference is that the second vortex has not formed even after the first vortex has detached (for $\tau > 3$) and moved well downstream. A good illustration of this situation may be seen at $\tau = 5.5$ (figure 10*e*). However soon after this two new vortices form together on the surface of the cylinder above the x-axis ($\frac{1}{4}\pi < \theta < \frac{1}{2}\pi$). The one nearest the x-axis then detaches and starts to move downstream (figure 10*h*). At $\tau = 8.0$ the other vortex has not yet detached but now a new vortex has formed in the neighbourhood of $\theta = 0$. They ultimately coalesce and will detach to pass downstream as a single vortex.

The variation of vorticity over the surface of the cylinder is shown up to $\tau = 4$ for the case $\alpha = \frac{1}{2}$ in figure 11 (*a*) and for the case $\alpha = 1$ in figure 11 (*b*). It is clear from figure 11 (*a*) that the variation of wall skin friction in the separated region where the wall is moving upstream ($0 < \theta < 40°$) is different from that where the wall is moving in the downstream direction ($320° < \theta < 360°$). For the case illustrated by figure 11 (*a*) ($\alpha = \frac{1}{2}$) separation has started in both of these regions at $\tau = 2$. Separation in the region of the upstream-moving wall is clearly accompanied by a reversal of wall skin friction very similar to that which occurs in the case $\alpha = 0$ of symmetrical flow; but the situation in the region near the downstream-moving wall is more complicated.

In figures 12–15 some details of the variation of the lift and drag coefficients with τ for the case $R = 500$ are given. The results obtained from the numerical solutions at small values of τ are in good agreement with those obtained from the formulae (59)–(61). It may be noted that the friction drag calculated from the analytical and numerical solutions is in agreement for relatively large values of τ, as indicated by the typical results in figure 13. The major departure of the results of the numerical integrations from those obtained from the series in powers of τ as τ increases is in the pressure drag; this shows itself in the curves for the total drag (figure 12). The typical results for the lift coefficient given in figure 14 suggest that C_L is directly proportional to α over the whole range of τ considered, certainly for these small values of α. This is consistent with the analytical expression (60) which is valid for small τ.

The present numerical method can be used to integrate the equations of motion particularly well for high Reynolds numbers because of the employment of the

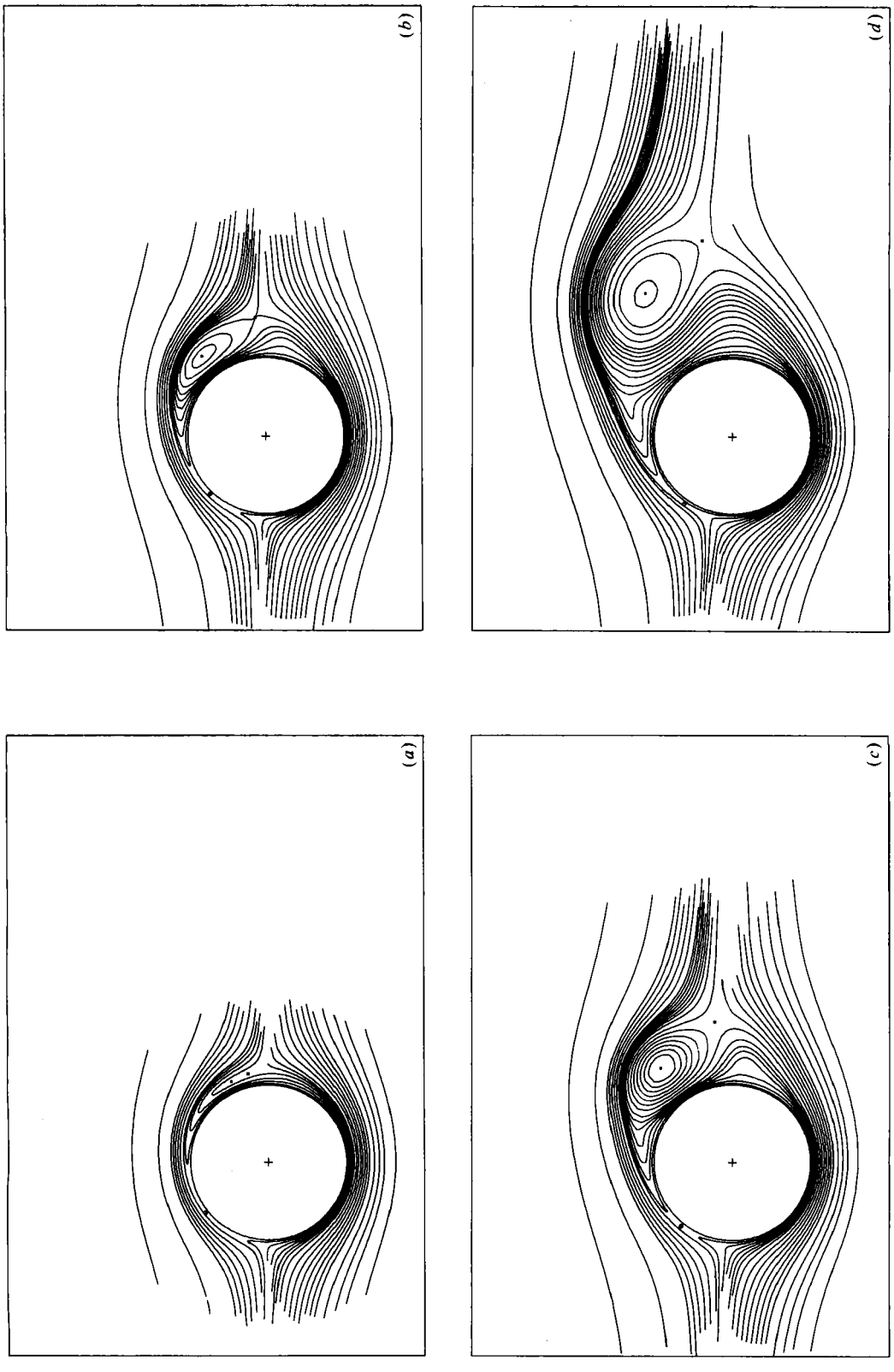

FIGURE 10 (*a*, *b*, *c*, *d*). For caption see page 482.

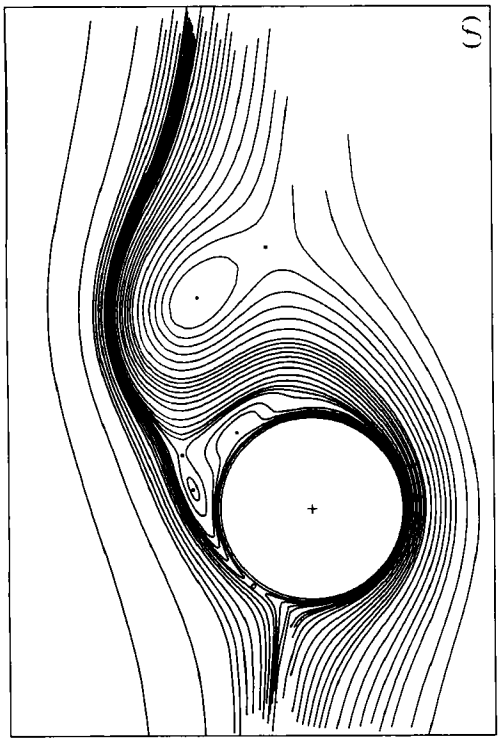

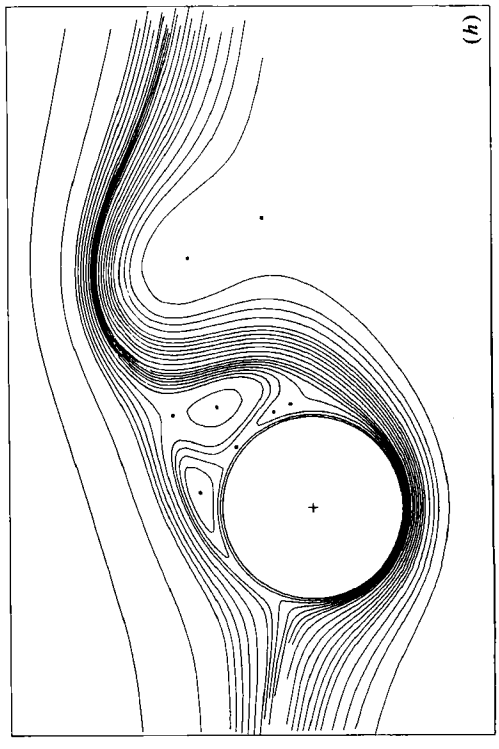

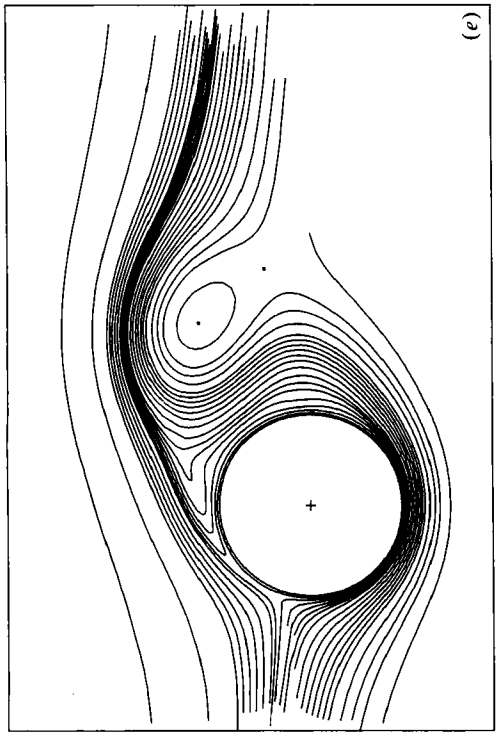

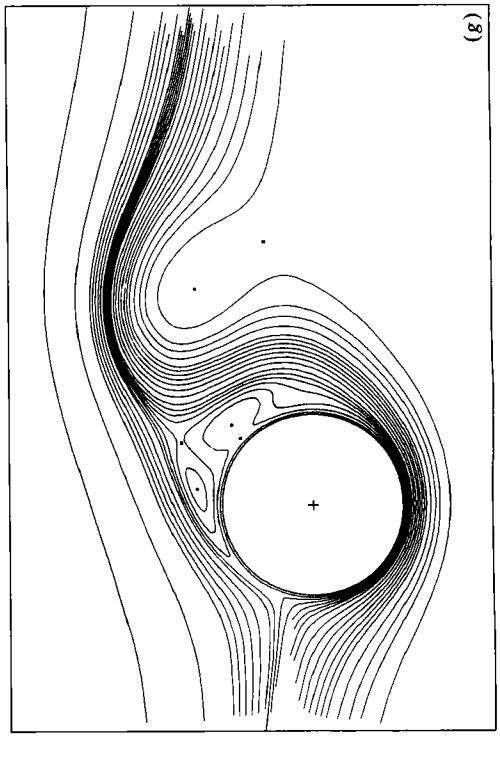

FIGURE 10 (*e, f, g, h*). For caption see page 482.

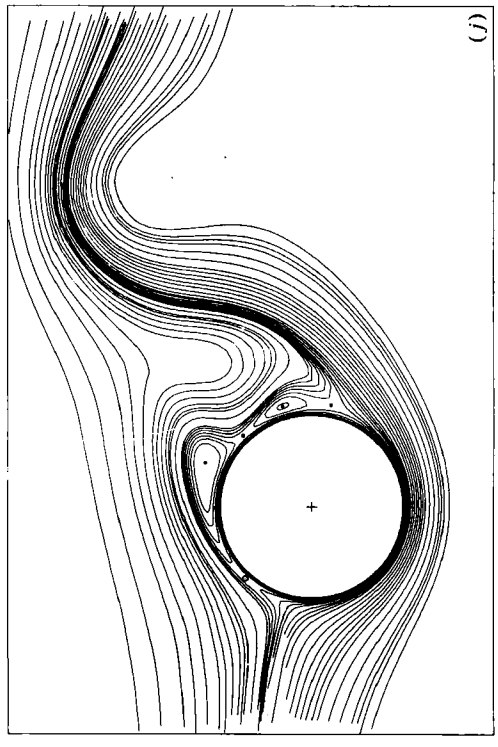

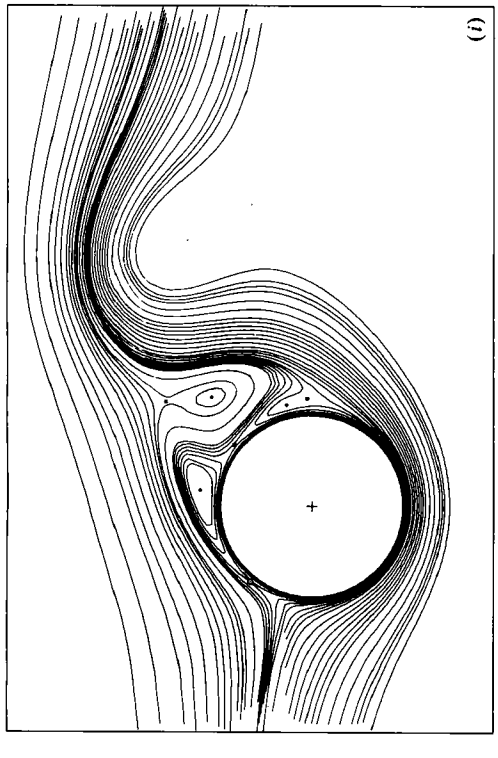

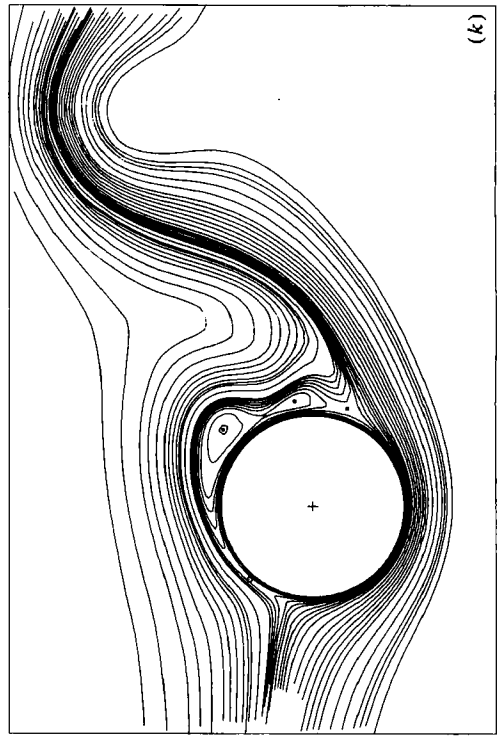

FIGURE 10 (i, j, k). For caption see page 482.

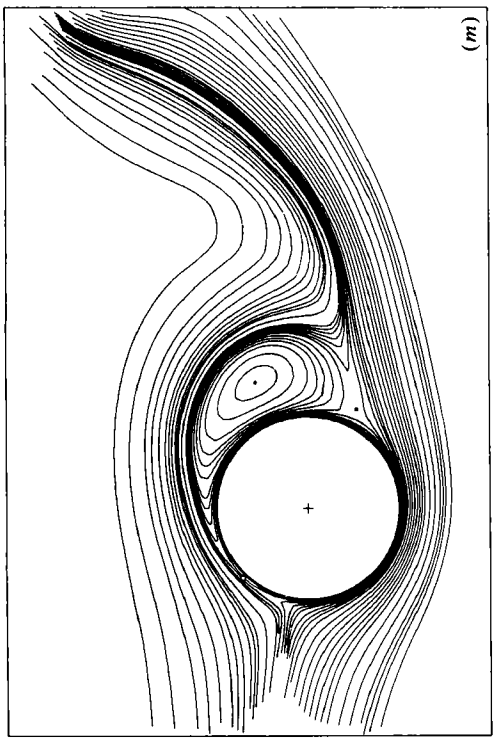

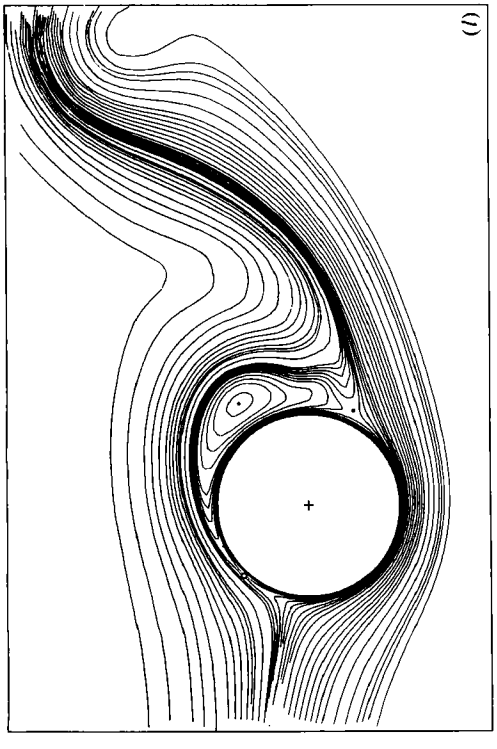

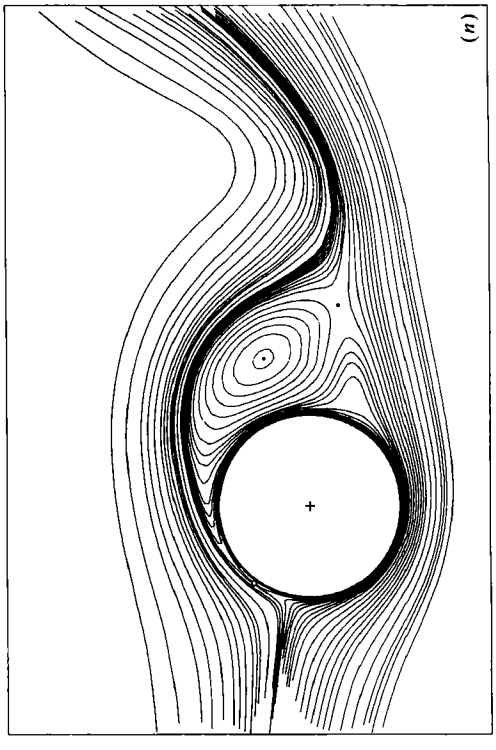

FIGURE 10. Instantaneous streamlines of the flow for $R = 500$, $\alpha = 1$ at various times: (*a*) $\tau = 1.0$; (*b*) 2.0; (*c*) 3.0; (*d*) 5.0; (*e*) 5.5; (*f*) 6.0; (*g*) 6.2; (*h*) 6.7; (*i*) 7.0; (*j*) 8.0; (*k*) 9.0; (*l*) 10.0; (*m*) 11.0; (*n*) 12.0. The streamlines in (*a*)–(*h*) correspond to the same values of ψ as those in figure 9(*a*)–(*e*) (extra streamlines $\psi = 0.02$, -0.03, -0.05, -0.09, -0.90, -1.10, -1.30, -1.50 are included in (*f*)) and in (*i*)–(*n*) to ψ values in figures 9(*f*)–(*k*).

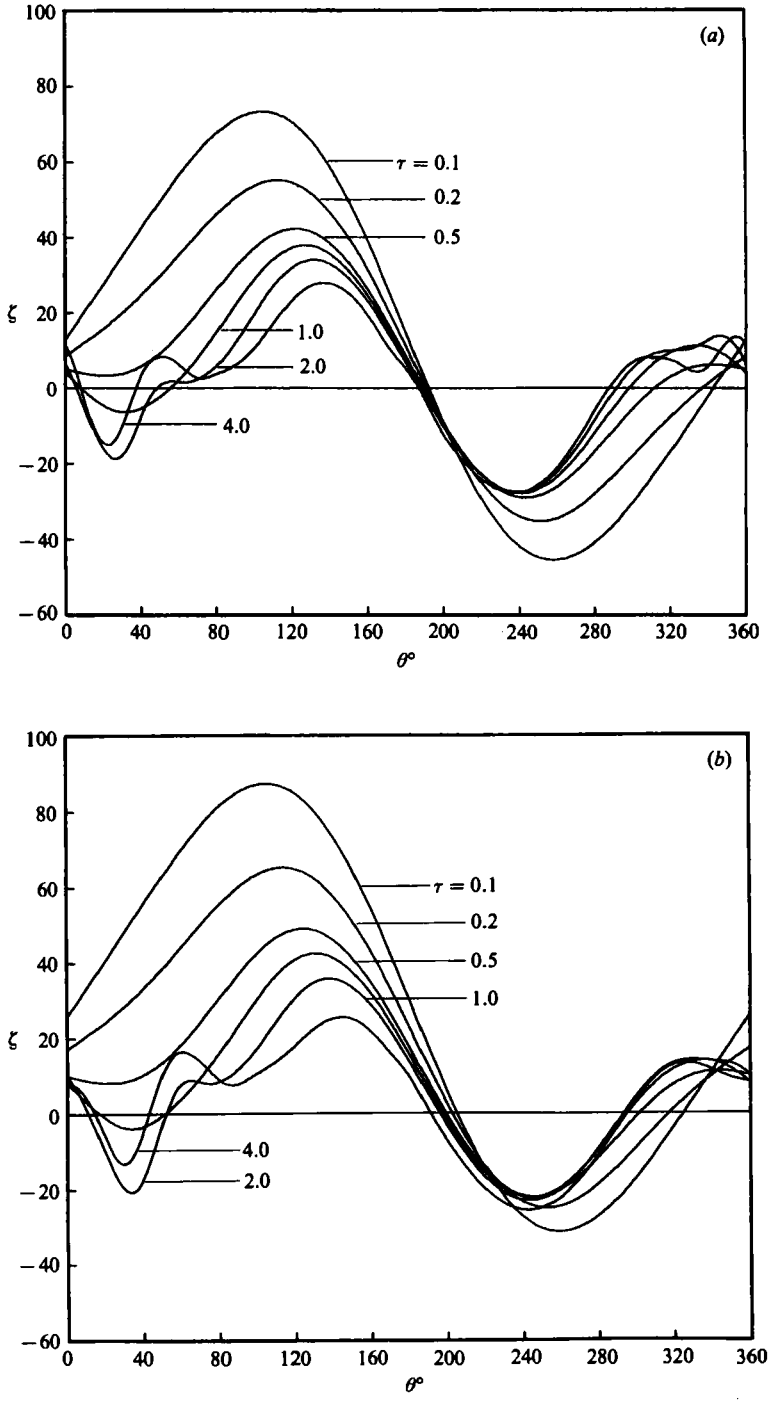

FIGURE 11. Evolution of the vorticity distribution on the surface of the cylinder at early times for $R = 500$ in the cases (*a*) $\alpha = \frac{1}{2}$; (*b*) 1.

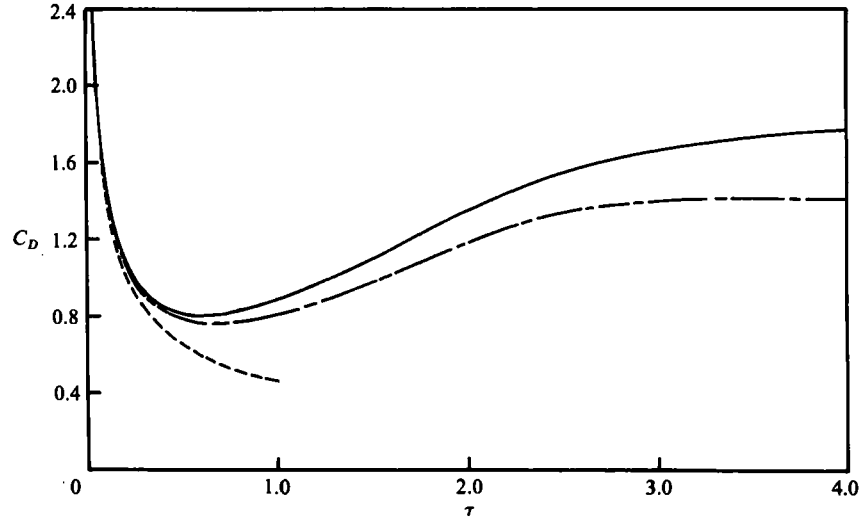

FIGURE 12. Variation of the drag coefficient with time at early times for $R = 500$: ——, numerical solution for $\alpha = 1$; – – – –, numerical solution for $\alpha = \frac{1}{2}$; – – – –, analytical solutions.

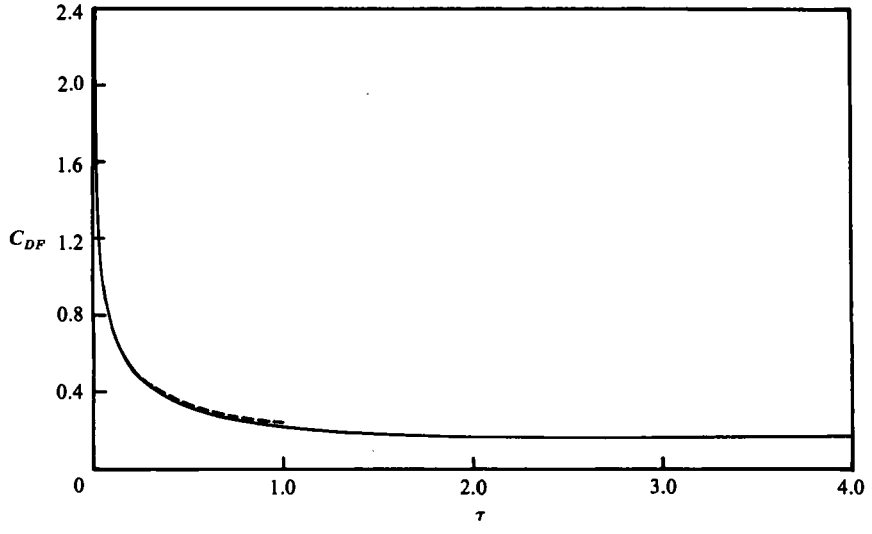

FIGURE 13. Variation of the frictional drag coefficient with time for the case $R = 500$, $\alpha = 1$: ——, numerical solution; – – – –, analytical solution.

boundary-layer coordinates. Some results are given for the vorticity on the surface of the cylinder and the lift, drag and moment in the limiting case $R \to \infty$ for $\alpha = 1$; these are shown in figures 16 and 17. In figure 17 the results of the numerical computations are compared with the limiting results of the series solutions as $R \to \infty$ obtained from (59)–(61). It is easily verified that the limiting forms of these equations when $\lambda = 0$ are

$$R^{\frac{1}{2}}C_D \sim \left(\frac{8\pi}{\tau}\right)^{\frac{1}{2}}, \quad R^{\frac{1}{2}}C_L \sim \alpha\left(\frac{128\tau}{9\pi}\right)^{\frac{1}{2}}, \quad R^{-\frac{1}{2}}C_M \sim (8\pi\tau)^{-\frac{1}{2}}, \tag{62}$$

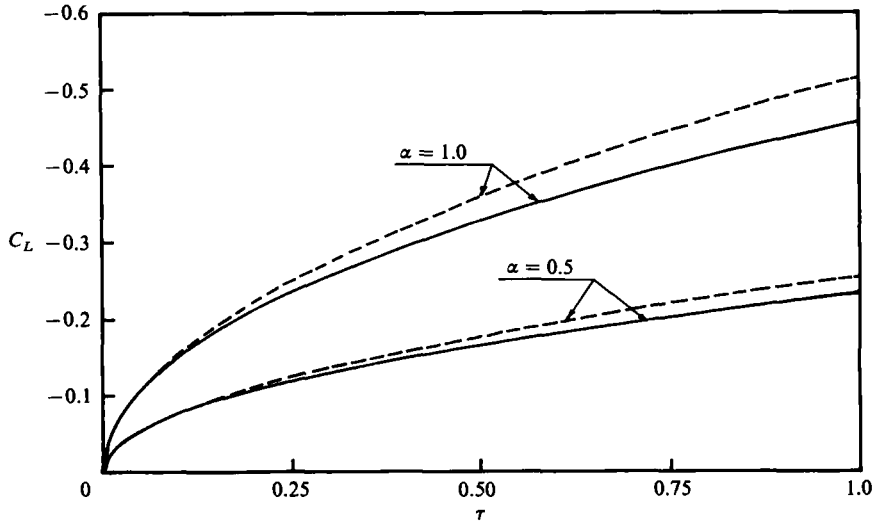

FIGURE 14. Variation of the lift coefficient at small times for the case $R = 500$: ——, numerical solutions; – – –, analytical solutions.

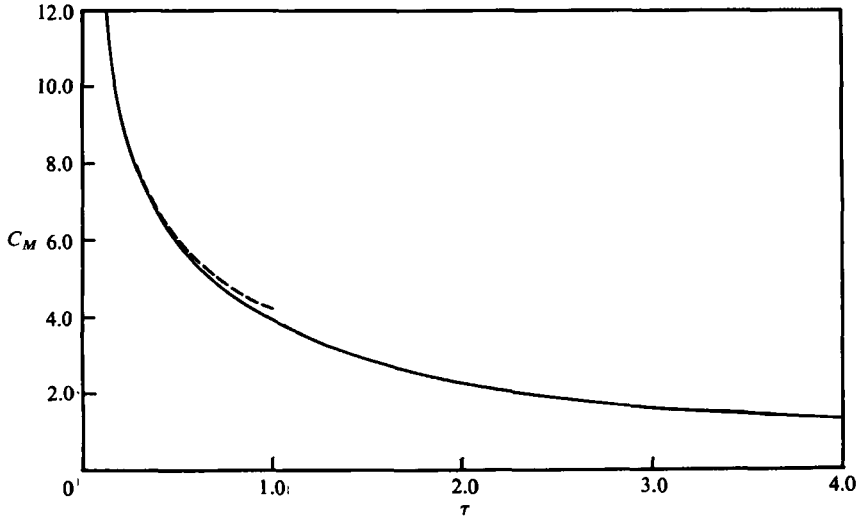

FIGURE 15. Variation of the moment coefficient at small times for $R = 500$, $\alpha = 1$: ——, numerical solutions; – – –, analytical solution.

as $R \to \infty$. The comparison is extremely good at small times. It is not possible to give streamlines of the flow because the calculations are carried out in boundary-layer coordinates and, since R is infinite, the actual physical distance from the surface of the cylinder to the edge of the boundary layer is zero. It is also not possible to integrate the boundary-layer equations to very large values of τ in this case $R \to \infty$ and at the same time maintain reasonable accuracy. A similar situation was found by Collins & Dennis (1973*b*) in the symmetrical case $\alpha = 0$. More recent work on this symmetrical boundary-layer problem such as that summarized, for example, by Cowley (1983) indicates that a singularity develops after a finite value of τ; it is extremely likely that a similar situation occurs in the present case.

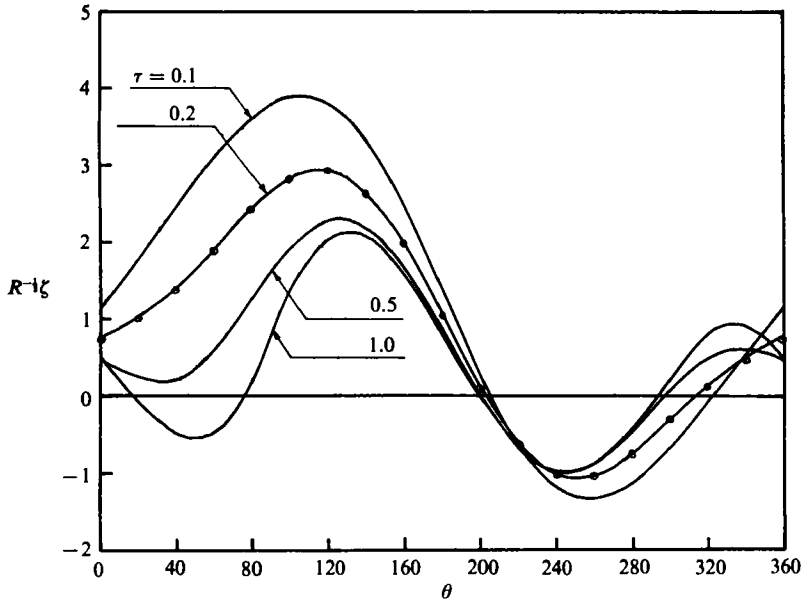

FIGURE 16. Evolution of the vorticity distributions on the surface of the cylinder at early times for the limiting case $R \to \infty$ when $\alpha = 1$: ——, numerical solution; ⊙, analytical solution at $\tau = 0.2$.

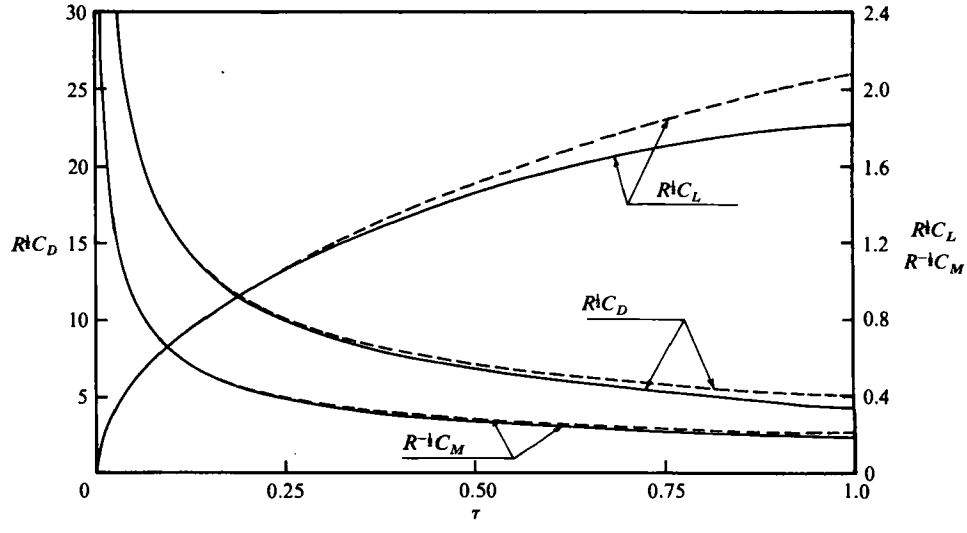

FIGURE 17. The variation of lift, drag and moment coefficients at early times for the limiting case $R \to \infty$ when $\alpha = 1$: – – –, analytical solution; ——, numerical solution.

In all cases of the flow which have been studied in the present paper there is one stagnation point in the fluid which forms soon after the start of the motion and then moves to a position which remains approximately stationary with time. This is the point near the upstream wall of the cylinder for $y > 0$ which is clearly shown for the case $R = 200$ in figures 1 and 2. In this case the experiments of Coutanceau & Ménard (1985) also show clearly the formation of this stagnation point and also the fact that after some preliminary movement its position subsequently remains constant with

	$\alpha = 0.5$		$\alpha = 1.0$	
τ	r/a	θ^0	r/a	θ^0
1	1.023	125.1	1.044	128.1
2	1.027	129.6	1.054	134.4
3	1.030	132.3	1.065	138.0
4	1.034	133.5	1.078	139.7
5	1.037	134.5	1.091	140.2
6	1.041	134.6	1.101	139.4
7	1.045	134.7	1.106	136.4
8	1.045	134.6	1.102	136.5

TABLE 1. Location of the front stagnation point for the cases of $R = 200$, $\alpha = 0.5$ and 1.0

time. In the case $R = 200$ the present calculations agree extremely well with the measurements reported by Coutanceau & Ménard. For example, for $\alpha = 1$ they report that the distance of this stagnation point radially from the cylinder surface stabilizes at about 0.1 radii for $\tau \geqslant 2$ and that as τ increases from about $\tau = 2$ to $\tau = 8$ the angular coordinate of the stagnation point decreases from about $\theta = 137°$ to $\theta = 131°$. Some results obtained from the present calculations are shown in table 1.

Finally, we may restate the conditions which have been assumed for the flow outside the boundary layer and near wake in the present calculations. At all stages of the motion a contour of sufficiently large radius surrounding the cylinder has been taken such that, at the time of termination of the calculations, the circulation round this contour remains zero, as it was at the start. The zero circulation has been enforced on the solution by satisfying (14), in particular (14*a*). The satisfaction of these global conditions is believed to be a more appropriate method than satisfying a condition imposed at the edge of the boundary layer since they are not dependent upon conditions enforced at one particular location of ξ. The work of Ingham (1983) in the case of steady flow past a rotating cylinder shows quite clearly how properties calculated from the solution can vary considerably depending upon the assumptions for the external flow. In the case of steady flow there is, of course, a circulation round a contour surrounding the cylinder and at large distances from it. The problem of specifying this circulation is avoided in the present work; in any case the solutions presented do not tend to a steady state. Nevertheless the imposition of boundary conditions in the numerical procedure which ensure that all the necessary conditions of the problem are satisfied, such as the required periodicity of the pressure, seems basic to the work. Similar problems do not usually arise in analytical methods.

The support of the Natural Sciences and Engineering Research Council of Canada for this investigation is gratefully acknowledged. One of us (S.C.R.D.) acknowledges support for a Canada–France exchange (administered by the National Research Council of Canada) which allowed contact with the personnel of the Laboratoire de Mécanique des Fluides, Université de Poitiers, during the course of their experiments. Many fruitful discussions with Dr Madeleine Coutanceau and her colleagues are acknowledged. Assistance with plotting routines at The University of Western Ontario by Mrs J. Winter and Mr L. White is also acknowledged. Finally, we gratefully acknowledge the interest and support of the University of Petroleum and Minerals, Dhahran.

REFERENCES

BADR, H. M., COUTANCEAU, M., DENNIS, S. C. R. & MÉNARD, C. 1985 *C.R. Acad. Sci. Paris.* **300**, série II, 529.

BADR, H. M. & DENNIS, S. C. R. 1981 In *Proc. 8th Canadian Congress of Applied Mechanics*, vol. 2, p. 659.

BATCHELOR, G. K. 1967 *An Introduction to Fluid Dynamics*. Cambridge University Press.

BLASIUS, H. 1908 *Z. angew. Math. Phys.* **56**, 1.

BOUARD, R. & COUTANCEAU, M. 1980 *J. Fluid Mech.* **101**, 583.

COLLINS, W. M. & DENNIS, S. C. R. 1973*a* *Q. J. Mech. Appl. Math.* **26**, 53.

COLLINS, W. M. & DENNIS, S. C. R. 1973*b* *J. Fluid Mech.* **60**, 105.

COUTANCEAU, M. & BOUARD, R. 1977*a* *J. Fluid Mech.* **79**, 231.

COUTANCEAU, M. & BOUARD, R. 1977*b* *J. Fluid Mech.* **79**, 257.

COUTANCEAU, M. & MÉNARD, C. 1985 *J. Fluid Mech.* **158**, 399.

COWLEY, S. J. 1983 *J. Fluid Mech.* **135**, 389.

DENNIS, S. C. R. & CHANG, G.-Z. 1969 *Tech. Summary Rep.* no. 859, Mathematics Research Center, U.S. Army, Madison, Wisconsin.

DENNIS, S. C. R. & STANIFORTH, A. N. 1971 In *Proc. 2nd Intl Conf. on Numerical Methods in Fluid Dynamics*. Lecture Notes in Physics **8**, 343. Springer.

GLAUERT, M. B. 1957*a* *Proc. R. Soc. Lond.* A **230**, 108.

GLAUERT, M. B. 1957*b* *J. Fluid Mech.* **2**, 89.

GOLDSTEIN, S. & ROSENHEAD, L. 1936 *Proc. Camb. Phil. Soc.* **32**, 392.

INGHAM, D. B. 1983 *Computers & Fluids* **11**, 351.

INOUE, O. 1981 *AIAA J.* **19**, 1108.

KOROMILAS, C. A. & TELIONIS, D. P. 1980 *J. Fluid Mech.* **97**, 347.

LUDWIG, G. R. 1964 *AIAA Paper* 64-6.

MOORE, D. W. 1957 *J. Fluid Mech.* **2**, 541.

MOORE, F. K. 1958 On the separation of the unsteady laminar boundary layers. In *Boundary Layer Research*, p. 296. Springer-Verlag.

PATEL, V. A. 1981 *Computers & Fluids* **9**, 435.

PRANDTL, L. 1925 *Naturwissenschaften* **13**, 93.

PRANDTL, L. & TIETJENS, O. G. 1934 *Applied Hydro- and Aeromechanics*. Dover.

RILEY, N. 1975 *SIAM Rev.* **17**, 274.

ROTT, N. 1956 *Q. J. Appl. Math.* **13**, 444.

SEARS, W. R. 1956 *J. Aero. Sci.* **23**, 490.

SEARS, W. R. & TELIONIS, D. P. 1975 *SIAM J. Appl. Maths* **28**, 215.

STANIFORTH, A. N. 1973 Ph.D. Thesis, University of Western Ontario.

TA PHUOC LOC 1975 *J. Méc.* **14**, 109.

TANEDA, S. 1977 *Prog. Aero. Sci.* **17**, 287.

TELIONIS, D. P. 1981 *Unsteady Viscous Flows*. Springer-Verlag.

THOMAN, D. C. & SZEWCZYK, A. A. 1966 *Tech. Rep.* 66–14. Heat Transfer and Fluid Mechanics Laboratory, Department of Mechanical Engineering, University of Notre Dame, Indiana, U.S.A.

TOLLMEIN, W. 1924 Dissertation, Göttingen.

WILLIAMS, J. C. 1977 *Ann. Rev. Fluid Mech.* **9**, 113.

WOOD, W. W. 1957 *J. Fluid Mech.* **2**, 77.